Title

Importance of global spherical geometry for studying slab dynamics and evolution in models with data assimilation

Authors

Peng, Diandian

Liu, Lijun

Publication Date

2023-06-01

DOI

10.1016/j.earscirev.2023.104414

Peer reviewed

Earth-Science Reviews 241 (2023) 104414

Contents lists available at ScienceDirect

Earth-Science Reviews

journal homepage: www.elsevier.com/locate/earscirev

Importance of global spherical geometry for studying slab dynamics and evolution in models with data assimilation

Diandian Peng [a,b,*], Lijun Liu [b,c,**]

[a] Institute of Geophysics and Planetary Physics, Scripps Institution of Oceanography, University of California, San Diego, La Jolla, CA, USA
[b] Department of Geology, University of Illinois Urbana-Champaign, Urbana, IL, USA
[c] State Key Laboratory of Lithospheric Evolution, Institute of Geology and Geophysics, Chinese Academy of Sciences, Beijing, China

ARTICLE INFO

Keywords:
Subduction
Mantle flow
Global model
Regional model
Data assimilation

ABSTRACT

Numerical modeling of subduction has proved increasingly important in understanding the evolution of Earth's internal dynamics and surface tectonic responses. A key criterion in judging models is their capability in matching both past plate tectonic constraints and the present-day mantle structures. In the past decades, most such models covered a regional mantle domain due to computational costs, while only recently sophisticated global spherical simulations became possible. Here we evaluate the effects of chosen model domain and applied boundary conditions in regional simulations on their resulting model results, by comparing them with more natural global simulations. All these models are based on the same sequential data-assimilation method and adopt the same plate tectonic history as surface boundary conditions. The only difference is that the regional models cover different geographic regions, representing a subset of the global one that covers the entire Earth. Besides illustrating the general impacts of chosen model setup on the resulting mantle evolution, we also make suggestions on the applicability of using regional models to replicate past subduction in four major circum-Pacific regions. The results show that the slabs from the global model match seismic tomography much better than the regional results in East Asia and South America; the main reason is that the regional models prohibit large-scale mantle flow as that in the global case, due to the non-penetrating side walls cutting off far-field forces. This limitation of regional models cannot be resolved by varying the model domain. In contrast, for North America and Fiji-Tonga, global and regional models produce similar slab structures, both matching tomography. This reflects that their fast-retreating overriding plates play an important role on the regional mantle flow and slab dynamics.

1. Introduction

Earth's dynamic evolution is, by definition, a time-dependent global-scale system. Geophysicists have made great progress in measuring Earth internal structures and their tectonic associations. For example, tomographic methods have helped to reveal otherwise unknown mantle structures (Obayashi et al., 2013; Ritsema et al., 2011), with fast seismic anomalies usually interpreted as being cold (e.g., the subducted slabs) while slow anomalies as being hot (e.g., the upwelling plumes). However, understanding the mechanisms and dynamics of these structures is not always straightforward. For instance, although consistently revealed by multiple tomography studies (Fukao et al., 1992; Huang and Zhao, 2006; Li et al., 2008), the formation mechanism of the >1500 km long stagnant slabs beneath East Asia have been heavily debated, ranging from vertical resistance due to mantle viscosity (Christensen and Yuen, 1985; Mao and Zhong, 2018) or slab buoyancy (King et al., 2015), to trench retreat (Christensen, 1996), and to lateral mantle flow (Peng et al., 2021a). Geological observations can provide temporal constraints, like the uplift and subsidence history of surface topography (Gurnis et al., 1998; Liu, 2015; Pang and Nummedal, 1995) and plate reconstructions based on different types of data (Müller et al., 2016; Torsvik et al., 2008). To construct the missing link between present-day mantle structures and geological events back in time while revealing physical mechanisms, numerical modeling of mantle convection

* Corresponding author at: Institute of Geophysics and Planetary Physics, Scripps Institution of Oceanography, University of California, San Diego, La Jolla, CA, USA.
** Corresponding author.
E-mail addresses: d3peng@ucsd.edu (D. Peng), ljliu@illinois.edu (L. Liu).

https://doi.org/10.1016/j.earscirev.2023.104414
Received 6 November 2022; Received in revised form 31 January 2023; Accepted 3 April 2023
Available online 6 April 2023

represents an increasingly important approach.

During the past decades, different types of mantle convection models have been developed, with progressively sophisticated model setups. Due to the limited computational power, early studies mostly utilized 2D or 3D regional-scale models. These models are flexible and computationally cheap, but usually simplified in geometry and boundary conditions. Many such 2D models were widely used to study different aspects of subduction, including the slab geometry with different mantle viscosity structures (Christensen, 1996; Gurnis and Hager, 1988), subduction initiation (Billen and Hirth, 2005; Leng and Gurnis, 2015), plume-slab interaction (Pusok and Stegman, 2020) and slab deformation and segmentation (Gerya et al., 2021). However, 2D models cannot reproduce complex 3D dynamics, such as the along-trench slab dip angle variation and toroidal mantle flow affecting slab evolution.

3D models, on the other hand, can generate these complex mantle features. These models can be either generic or Earth-like. For example, generic 3D regional models were used to study the effects of trench width on slab evolution (Schellart et al., 2007; Stegman et al., 2006), and generic global models were useful to understand the dynamics of supercontinent cycles (Zhong et al., 2007). Earth-like models are among the most recent efforts of better reproducing realistic Earth processes, with common approaches including the forward-in-time sequential (Bower et al., 2015; Bunge et al., 1998; Hu et al., 2018; Liu and Stegman, 2011) and back-in-time variational (Bunge et al., 2002; Ismail-Zadeh et al., 2004; Liu and Gurnis, 2008; Liu et al., 2008) data-assimilation schemes. These models usually absorb as boundary conditions the rich information from recent plate reconstructions which cover plate kinematics and other tectonic information back to hundreds of millions of years ago (Müller et al., 2016; Torsvik et al., 2008). Variational models further take advantage of mantle seismic images as model inputs. By directly connecting past plate tectonics with mantle convection, we can use these models to provide detailed 3D slab evolution and mantle thermal structures that match independent geological and geophysical observations, thus providing important insights on the behaviors of mantle plumes and subduction (Zhou and Liu, 2017; Hassan et al., 2016; Hu et al., 2016; Liu and Stegman, 2011; Mao and Zhong, 2018; Peng et al., 2021a).

Although vastly useful, the different types of numerical models also lead to controversies, such as the aforementioned stagnant slab formation. We suggest that these are due to intrinsic differences among these models that affect the results differently. First, 2D models are unable to represent 3D mantle flow and structures as discussed before. Second, regional models in both 2D and 3D usually have reflective side boundaries while global models do not. These model limitations were traditionally justified by the intent of studying certain scenarios, including a long subduction zone with little along-strike variation (a 2D scenario) or a single isolated slab that has little interaction with other dynamic processes (a regional scenario). However, it is anticipated that the chosen boundary conditions for these regional models should strongly affect model results (Gurnis and Hager, 1988; Han and Gurnis, 1999; Zhong and Gurnis, 1995).

In addition, Earth's subduction systems are usually interconnected, implying slab interaction at depth (Pusok and Stegman, 2020). Consequently, mantle flow beneath a continental plate could be in the opposite direction to that of the surface motion, as is controlled by slabs within the lower mantle or below other subduction zones (Peng et al., 2021a). The existence of large low shear velocity provinces (LLSVP) that are of very-long wavelength (spherical harmonic degree 2) in the lower mantle would inevitably interact with many slabs, a process that is hard to be captured in regional models. These necessitate a re-evaluation of the effect of model domain and boundary conditions on the resulting slab dynamics and mantle flow, as is the purpose of this study.

Previous global models or large-scale regional models were limited by inadequate resolution in resolving subducting slabs due to the computational limitation. With increasing computational power, these models, including global ones, can now approach much higher resolution as that in recent regional models (Hu et al., 2016; Liu and Stegman, 2011). Consequently, it is possible to use global models to reproduce many key slab structures across mantle depths (Ma et al., 2019; Mao and Zhong, 2018; Peng et al., 2021a). In this study, we perform 3D (both global and regional) and 2D models with data assimilation and compare them with tomography results. We focus on four major subduction zones around the Pacific, located at the southwest (Fiji-Tonga), northeast (North America), southeast (South America) and northwest (East Asia). We compare these model results with tomography and discuss their differences. We deem this work to be timely, given that global 3D data-assimilation models are still computationally too expensive for many users. We provide some guidance on how to design regional models for a specific subduction problem.

2. Methods and model setup

In this study, we show the results of a global model and four regional models targeted on different subduction zones (Fig. 1), as well as some 2D models for East Asia. All models utilize the same plate reconstruction, thus keeping the consistency (unless specified) among them in terms of boundary conditions (top and bottom), background viscosity, temperature profile and compositional properties. We utilize one global model (the Model 2 in Peng and Liu, 2022) and four regional models, tailored for Fiji-Tonga, North America, South America and East Asia, to compare their respective results for a common geographic region. We also performed four 2D models for East Asia with different model domains.

2.1. Governing equations

In this study, we run thermal-chemical models with sequential data assimilation (Hu et al., 2018; Liu and Stegman, 2011; Peng et al., 2021a, 2021b) from 200 *Ma*. The mantle is assumed to be incompressible and satisfies the Boussinesq approximation. We use the open-source mantle convection code CitcomS with spherical coordinates (McNamara and Zhong, 2004; Tan et al., 2006; Zhong et al., 2008). The equations for the conservation of mass, momentum and energy and the advection of chemical tracers are:

$$\nabla \bullet \vec{u} = 0, \tag{1}$$

$$-\nabla P + \nabla \bullet \left[\eta\left(\nabla \vec{u} + \nabla^T \vec{u}\right)\right] + \left(\rho_m \alpha \Delta T + \Delta\rho_c\right)\vec{g} = 0, \tag{2}$$

$$\frac{\partial T}{\partial t} + \vec{u} \bullet \nabla T = \kappa \nabla^2 T, \tag{3}$$

$$\frac{\partial C}{\partial t} + \vec{u} \bullet \nabla C = 0, \tag{4}$$

where $\vec{u}$ is the mantle flow velocity, P is the dynamic pressure, η is the dynamic viscosity, ρ_m is the density of the ambient mantle, α is the thermal expansion coefficient, ΔT is the temperature anomaly, $\vec{g}$ is the gravitational acceleration, C is composition and $\Delta\rho_c$ is the compositional density anomaly.

2.2. Setup of the global 3D model

The global model discretizes the mantle domain into 12 spherical caps, each having 257 × 257 × 113 nodes. The horizontal resolution is ~23 km at the surface and ~ 12 km at the core-mantle boundary (CMB). The vertical resolution is ~12 km near the surface, ~26 km near the CMB, and ~ 31 km in the mid-mantle. In order to adequately capture the evolving slab geometry with the finite numerical resolution in a global model like this, we use a reduced Rayleigh number of 2.6×10^8 (scaled with Earth's radius instead of the model thickness) and a mantle temperature of 700 °C. To maintain the buoyancy of the oceanic plate, we

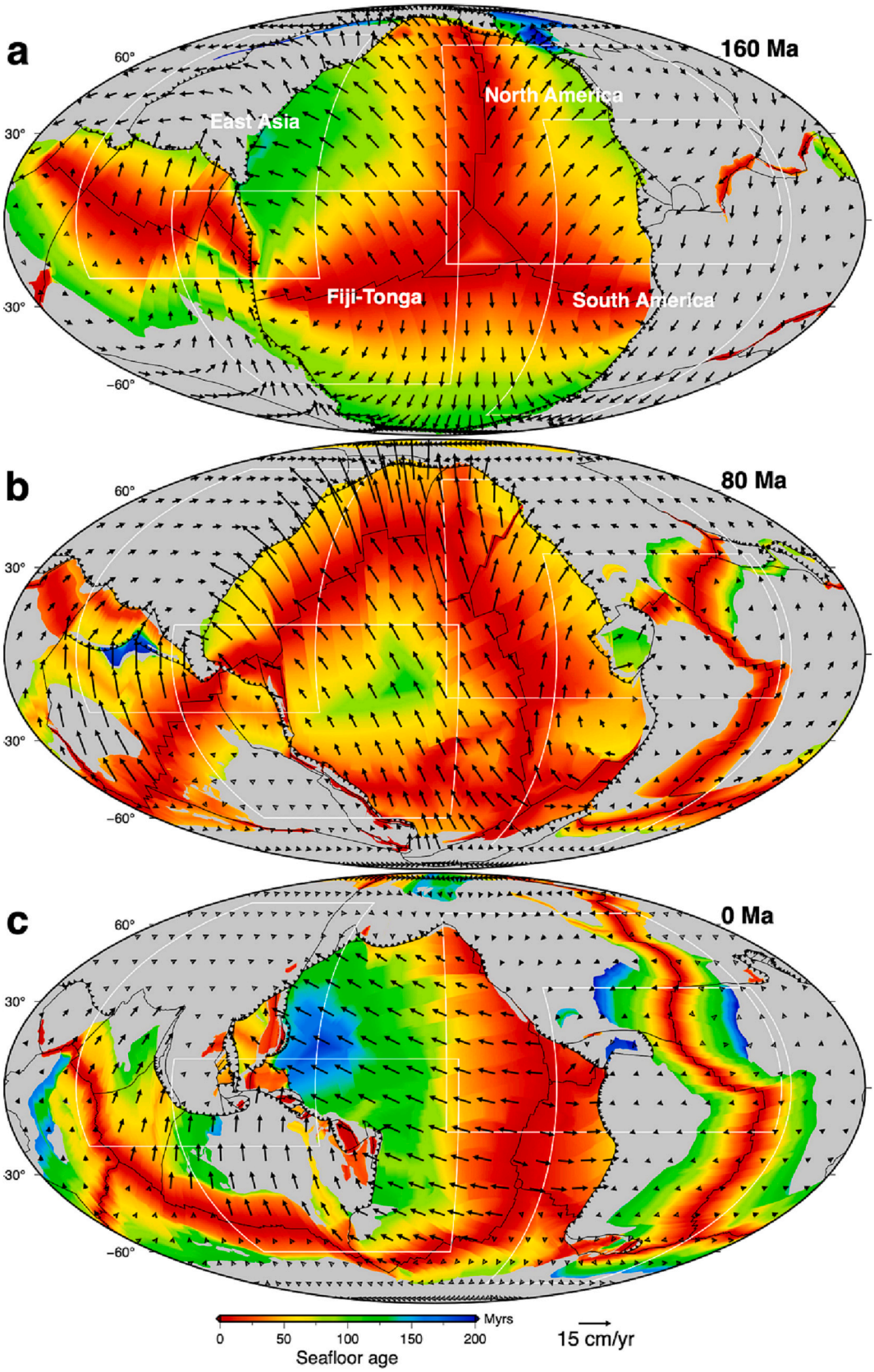

Fig. 1. Seafloor age and surface velocity at different geological times from plate reconstruction (Müller et al., 2016). The white boxes mark the domains of the four regional 3D models.

used a modified half-space cooling model for the oceanic lithosphere (Hu et al., 2018; Liu and Stegman, 2011), with the seafloor age (Fig. 1) adopted from a recent plate reconstruction (Müller et al., 2016). With this modification, we make sure that the buoyancy of the subducting plates is close to that in the real Earth, and the convection vigor in our model remains similar to studies with a larger temperature contrast (e.g., Mao and Zhong, 2018). Relative to most earlier data-assimilation models of its kind, our simulated slabs are naturally asymmetric at shallow depth and deform freely after entering the convective mantle. The model has a free slip bottom boundary, and the surface assimilates velocities (Fig. 1) from the plate reconstruction (Müller et al., 2016). The continents have a steady-state initial temperature profile. The viscosity structure depends on depth, temperature, and composition, with a layered background viscosity profile and a reference viscosity of 10^{21} Pas. There is a 250-km thick thermal-chemical layer defined as an initial condition to simulate the formation of the LLSVPs. This layer has higher temperature and lower viscosity than the ambient mantle. The chemical density anomaly is about 2.4%, consistent with previous studies (Hassan et al., 2016; Zhang and Li, 2018). More details about the model setup and parameters can be found in our previous studies (Peng et al., 2021a, 2021b; Peng and Liu, 2022).

2.3. Setup of the regional 3D models

The regional models differ from the global model mostly in terms of the horizontal dimensions and meshes. The mesh of each regional model has 257 × 257 × 113 nodes in the latitude×longitude×radius dimensions. Horizontally, the mesh is denser in the center than near the side boundaries. The vertical mesh resolution is the same as that in the global model. Different from the global case, the regional model has four side walls that are free to slip in the vertical direction. When assimilating the surface velocity as a boundary condition, the velocity is set to gradually vanish toward the edge within 10 nodes. Another difference is that the thermal-chemical piles (LLSVPs) above the CMB are not included in the regional models. One reason is that these hemispheric-scale structures cannot be formed in reginal models. Another reason is that for many regions with subduction (e.g., East Asia, North America), LLSVPs are not present above their respective CMB, but an initial thermal-chemical pile in the regional models will lead to wrong results because the deformed pile must stay in the model domain due to conservation of mass.

The Tonga model domain is 100° to 220° in longitude and − 60° to 10° in latitude. The resolution in the center is ~30 km north-south and ~ 43 km east-west. For most of the time since 200 *Ma*, the trench in the southwestern Pacific is located a long distance west of the present-day Tonga subduction zone (Fig. 1), until about 50 *Ma*. To be consistent with the global model, this regional model still starts from 200 *Ma*. The model domain is large enough to cover the ancient subduction zones along eastern Australia from 200 *Ma*.

The North America model domain is 215° to 355° in longitude and − 15° to 65° in latitude. The resolution in the center is ~35 km north-south and ~ 49 km east-west. It contains the subduction of the Farallon and Cascadian slabs beneath North America and the Cocos slab beneath Central America.

The South America model domain is 261° to 359° in longitude and − 75° to 35° in latitude. The resolution in the center is ~48 km north-south and ~ 37 km east-west. This model covers the subduction of the Farallon and Nazca slabs beneath South America.

The East Asia model domain is 60° to 160° in longitude and − 20° to 70° in latitude. The resolution in the center is ~39 km north-south and ~ 36 km east-west. This domain covers most of the northwestern Pacific subduction zone and part of the Tethyan subduction zone (including the Indian-Eurasia collision and the Sumatra-Java subduction) from 200 *Ma*.

2.4. Setup of the regional 2D models

Since 2D models still prevail in the recent literature, we also run some 2D models using the data-assimilation technique as in the regional 3D models. We design four 2D models in order to compare with the regional model for East Asia. These 2D models are along latitude 43°N, the cross-section commonly displayed in several of our previous papers (Liu et al., 2021b; Peng et al., 2021a, 2021b; Peng and Liu, 2022). The 2D models have only one element in the latitude direction. On the vertical direction, the meshes are the same as in the global and regional models. The longitude ranges are 100° to 160°, 60° to 160°, 40° to 180° and 40° to 220°, partitioned with 129, 257, 385 and 513 nodes, respectively. This results in horizontal resolutions of 35 km, 30 km, 29 km, and 28 km.

2.5. Quantitative comparison with tomography results

To evaluate the model results, we chose five tomographic models to compare with results from our mantle convection models. There are three P-wave models, UU-P07 (Amaru, 2007), MIT-P08 (Li et al., 2008), GAP-P4 (Obayashi et al., 2013) and two S-wave models, S40RTS (Ritsema et al., 2011) and SEMUCB-WM1 (French and Romanowicz, 2014). In addition to a direct comparison between the modeled slabs with those in tomography, we also quantified the match between modeled temperature structure with tomographic results by calculating the sensitivity and accuracy (Flament, 2019). The sensitivity is TP/(TP + FN) and the accuracy is (TP + TN)/A. TP (true positive) is the volume with high seismic velocity and low model temperature. FN (false negative) is the volume with high seismic velocity and high model temperature. TN (true negative) is the volume of low seismic velocity and high model temperature. A is the total volume. In this study we focus on the slabs which has cold temperate or fast seismic velocity, so sensitivity (decided TP and FN) is a better criterion than accuracy (also relys on the slow anomalies). As a reference, we also calculated the sensitivity between tomographic models. For the calculation, we avoid the 10 nodes close to the side boundaries within the regional models in the lateral directions. In the vertical direction, the depth range is chosen to include the major slabs observed by tomography. For comparison, the global model is tailored to the same domains as the regional ones.

3. Results

As shown in our previous studies, the global model properly reproduces the slab geometries along all major subduction zones (Peng et al., 2021a, 2021b; Peng and Liu, 2022). In this study, we mainly focus on the circum-Pacific subduction zones (Fig. 2). We first show the simulated present-day slabs in two view angles from the global model, focusing on the western Pacific (Fig. 2a) and eastern Pacific (Fig. 2b), respectively. The major slabs on the western side of the Pacific include the Pacific slab and the Philippine Sea slab subducted beneath East Asia, and Tonga slab subducted along the Tonga subduction zone. The Indian and Sumatra-Java slabs belong to the Tethyan subduction zone. On the eastern side of the Pacific, there are the Farallon slab beneath North America and South America, the Cocos slab beneath Central America and the Nazca slab beneath South America. The mantle beneath the Pacific is free of slabs where the LLSVP is present in the lower mantle that is not shown here (French and Romanowicz, 2014; Ritsema et al., 2011). Global scale evaluation of this global model and quantitative correlations with tomographic results can be found in Peng and Liu (2022), where we showed that both the cold anomalies in the upper mantle and hot anomalies in the lower mantle match tomography well. For spherical harmonic degree 1–8, the correlations with S-wave tomographic models are high, supporting the good match for long wavelength structures. Next, we will compare the mantle structures and slab dynamics in the global model with those from the regional models.

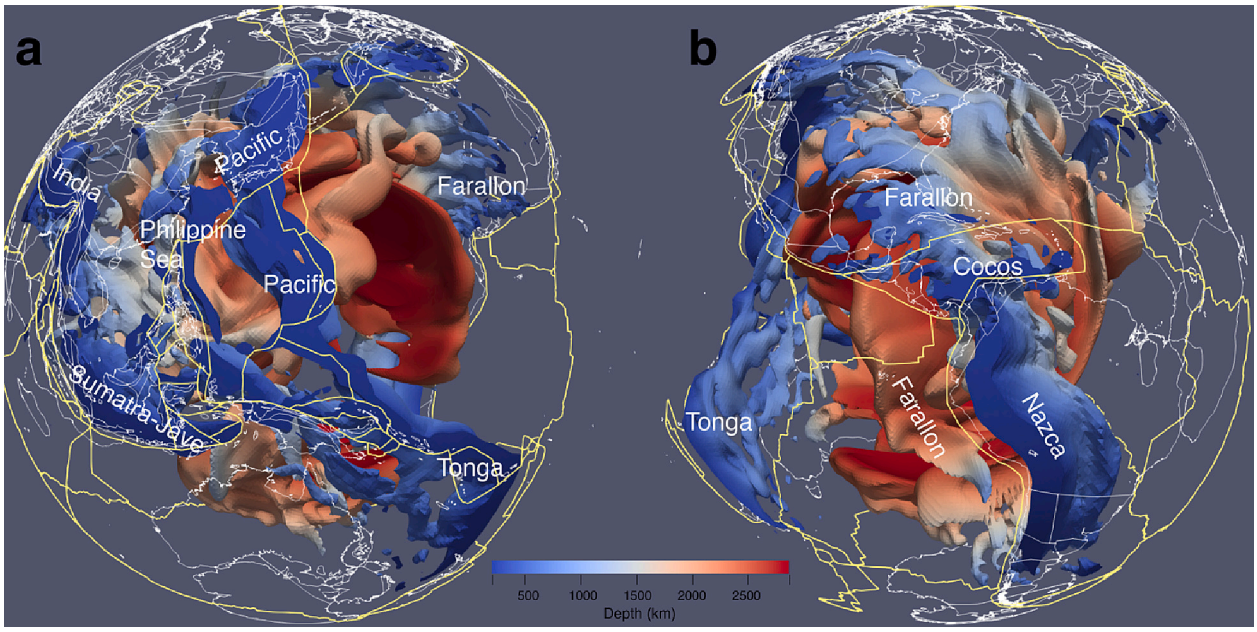

Fig. 2. The depth distribution of slabs in the global model with a western Pacific view (a) and eastern Pacific view (b). Slabs are defined with an isosurface of negative temperature anomaly at −250 °C (relative to the ambient mantle) with the colour showing their depths. On the surface the white lines show tectonic boundaries within continents and global coastlines. The yellow lines show plate boundaries. Major slabs are marked on the figure. (For interpretation of the references to colour in this figure legend, the reader is referred to the web version of this article.)

3.1. Fiji-Tonga

The Tonga subduction zone experienced the fastest trench retreat during the Cenozoic, with a rate up to 16 cm/yr (Schellart et al., 2007). The toroidal flow around the slab edge induced by the retreating slab may have entrained Samoan plume material into the spreading northern Lau Basin (Chang et al., 2016; Druken et al., 2014; Strak and Schellart, 2014). From 200 *Ma*, this region has been part of the Pacific Ocean, with no active subduction until ~50 *Ma* (Fig. 1). This explains the observation that there are not many deep slabs beneath Tonga (Fig. 3a,b). Both the global and regional models predict the stagnant Tonga slab which is also consistent with the tomographic images (Figs. 3, S1). The differences of slab geometries in these two models are minor. In the upper mantle depth range, the regional model has better sensitivities against tomography results than the global model (Fig. 3e). The prominently good match near 660 km marks the presence of stagnant slabs. Both

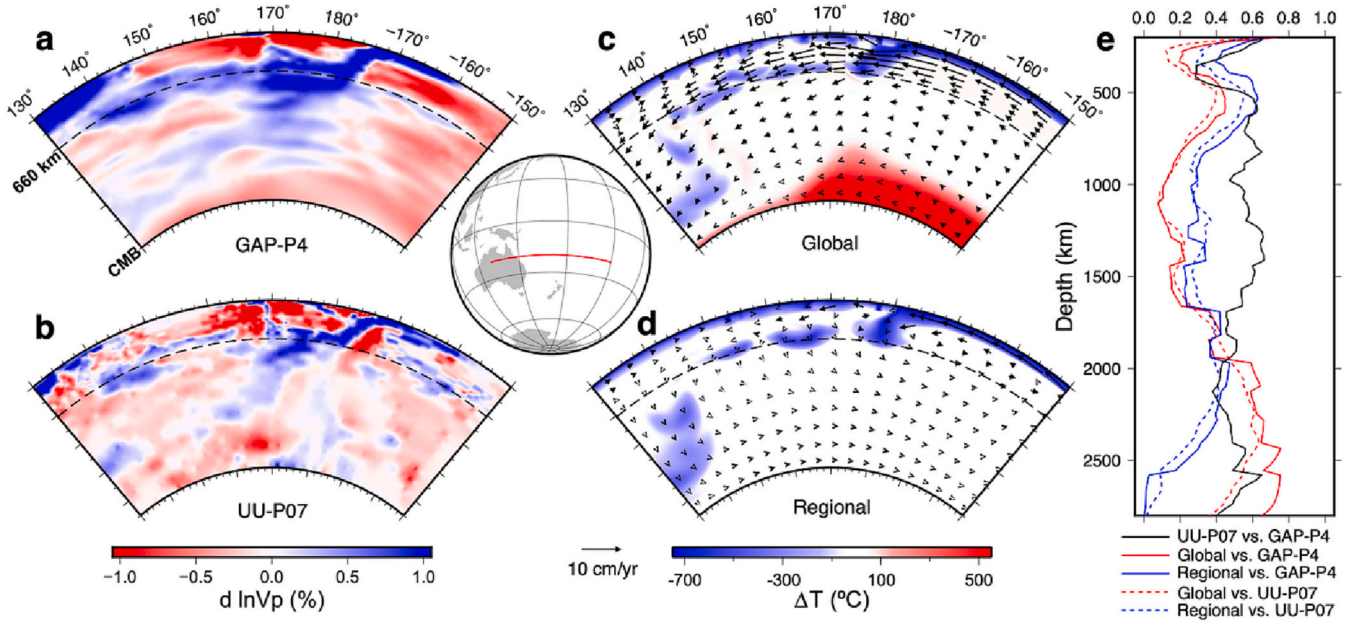

Fig. 3. Tonga slabs in tomography, the global model and the regional model. The panel in the center marks the cross-section of 20°S with the red line. (a,b) Seismic velocity anomalies in GAP-P4 and UU-P07, respectively. (c,d) Temperature anomalies and mantle flow in the global model and regional model, respectively. The dashed lines show the 660 km discontinuity. (e) Sensitivities of the global (red curves) and regional (blue curves) models against GAP-P4 and UU-P07. The sensitivity of UU-P07 against GAP-P4 is also shown (black curve) as a reference. The seismic velocity anomalies for the same cross-section are shown for MIT-P08, S40RTS and SEMUCB-WM1 in Fig. S1, along with the sensitivity and accuracy. (For interpretation of the references to colour in this figure legend, the reader is referred to the web version of this article.)

models have low sensitivity values in the mid-mantle because of this depth is free of slabs (Fig. 3c,d). Due to the lack of an initial thermal-chemical pile above CMB in the regional model, the sensitivity is low comparing to the global model (Fig. 3e). The volume weighted average sensitivity of the global and regional models against all the five tomographic results are summarized in Table S1.

Although the regional model does not incorporate a chemically dense hot basal chemical layer as in the global model (Fig. 3c), we do not observe any clear effect of this chemical layer in driving the lower-mantle flow, thus mantle structures. This supports the passive nature of the LLSVPs (McNamara, 2019; Reiss et al., 2019), where their compositional and thermal buoyancy offset each other. Indeed, the similar geometry of stagnant slabs in the two models suggest that the LLSVPs in the lower mantle have limited effect on the upper mantle slab structures.

The similar upper-mantle slab structures between global and regional models are also reflected in the similarity of dynamic pressure, where the most prominent difference is that the global model has a low-pressure zone in the lower mantle associated with the Pacific LLSVP (Fig. 4). Consequently, their velocity fields are also close to each other. The only notable difference is that the global model has a westward mantle flow in the upper mantle during the latest Cenozoic (Fig. 4c) while the regional model does not (Fig. 4f). This mantle flow may explain why the stagnant slab in the global model is slightly longer and more continuous than in the regional model, but is not the key mechanism for the slab stagnation. The upper mantle velocities beneath the Pacific Plate demonstrate a typical Couette-type flow in the global model, but this flow is weaker in the regional model, where the mantle transition zone (MTZ) depth even hosts as an eastward return flow in the opposite direction of plate motion. This difference represents an artifact due to the side boundaries of the regional model.

Overall, the global and regional models result in similar present-day stagnant Tonga slab. We suggest this reflects the dominant effect of trench retreat on the formation of this characteristic slab structure (Goes et al., 2017; van der Hilst and Seno, 1993) instead of regional mantle wind as proposed for the stagnant slabs beneath East Asia (Peng et al., 2021a). Although there are clear differences in the mantle flow between the two models, these differences occurred mainly toward the present day, and thus should have not affected the slab geometry due to the short duration when they played a role. Another possible reason for the similar slab structures is that Tonga subduction zone has a short subduction history (since 50 *Ma*) and is not limited by the effect of previous subduction (Peng et al., 2021a, 2021b). Consequently, this comparison implies that regional models could correctly reproduce the subduction history of the region.

3.2. North America

The Farallon slab, originally subducted along the west coast of North America (Müller et al., 2016), now lies beneath central to eastern North America in the lower mantle (Grand et al., 1997; van der Meer et al., 2010). Interpretation on the location of this slab relative to that of North

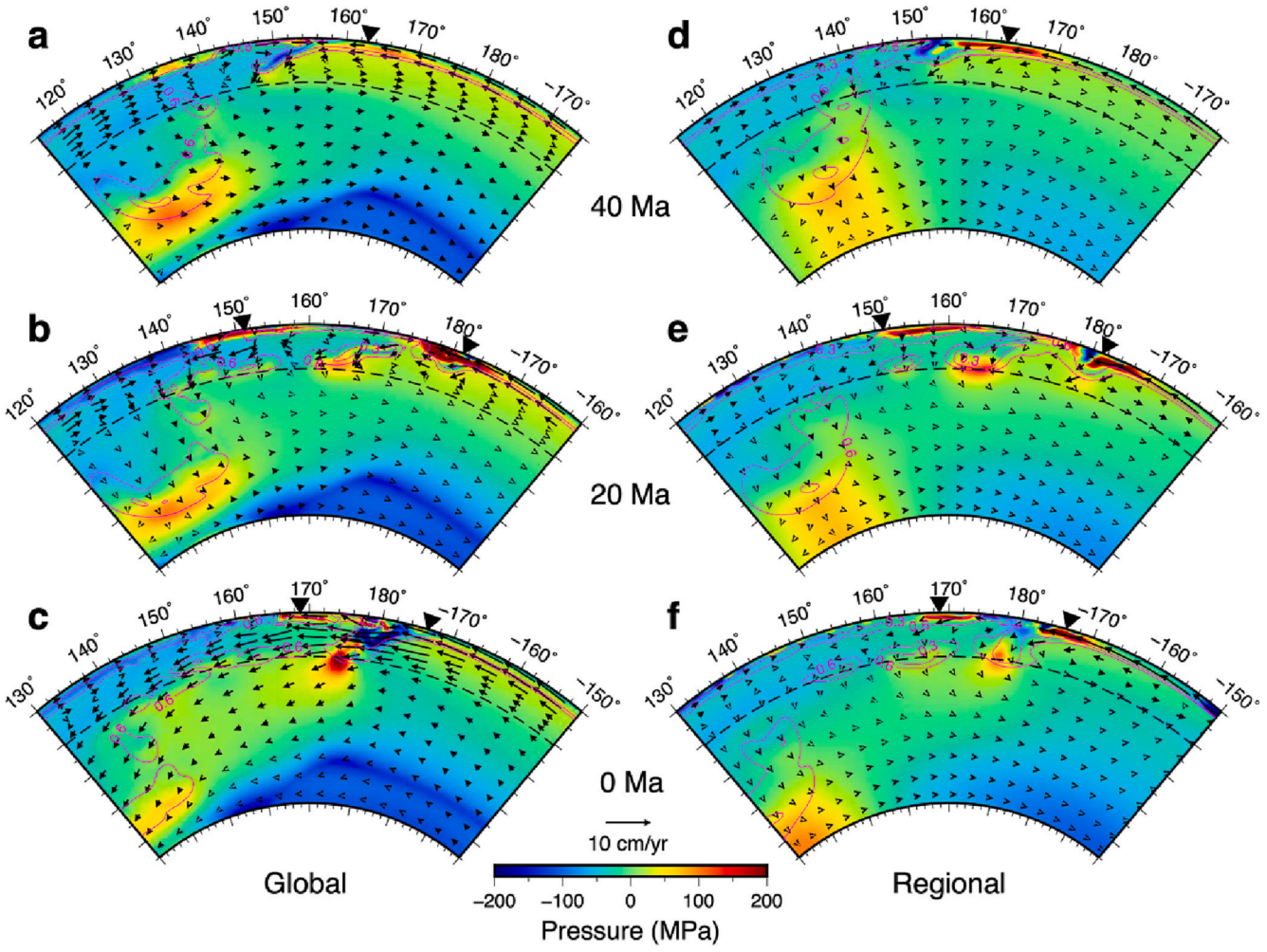

Fig. 4. The evolution of slabs, dynamic pressure, and velocity field beneath Tonga along 20°S. (a-c) Global model evolution with time snapshots at 40 *Ma*, 20 *Ma* and 0 *Ma*, respectively. (d-f) The same as (a-d) but for the regional model. The black triangles mark the trench locations.

America has led to models of intra-ocean subduction with vertically sinking slabs during the Mesozoic (Sigloch and Mihalynuk, 2013; van der Meer et al., 2010) and eastward migration of the subducting Farallon slab in the mantle (Liu, 2014; Peng and Liu, 2022). A stagnant portion of the Farallon slab at shallow depth is also recognizable in the uppermost lower mantle (Goes et al., 2017). Besides the observed geometry of the Farallon slab, another important aspect is the flat subduction (Bird, 1988; Humphreys, 1995; Liu et al., 2008). A flat Farallon slab as traditionally proposed may have contributed to multiple geological features and events including the present-day lithospheric structure (Bird, 1988), the elevation of Laramide province (English et al., 2003; Humphreys, 1995; Saleeby, 2003), the migratory magmatic arc (Coney and Reynolds, 1977; Liu et al., 2021a), and the temporal evolution of surface topography (Heller and Liu, 2016; Liu et al., 2008). Therefore, in addition to the present-day slab structures, a reasonable subduction model should also reproduce this Mesozoic flat Farallon slab.

At the present-day, tomographic results show a dipping Farallon slab from the western or middle North America in the upper mantle to the east coast in the lower mantle (Figs. 5a,b, S2). We find that the major features of the Farallon slab are appropriately reproduced in both the global and regional models, with similar slab configuration (Fig. 5c,d). However, the slab in the regional model is slightly eastward shifted and has a shallower depth (Figs. 5b, 6), while the global model fits tomography better (Fig. 5). The match to tomography is low for both models in the shallowest mantle, likely due to the complex lithospheric structures absent in the geodynamic models (Fig. 5e). In the lower mantle, the global model shows a better fit. Overall, the global model predicts the Farallon slab better than the regional model but only marginally. The major difference is mainly because of the eastward shifted Farallon slab in the regional model that misses the seismic slab (Fig. 6).

In the cross-sectional view, these two models have similar flow patterns in the upper mantle throughout the simulation (Fig. 7). Toward the present, both models generate an eastward flow originating from the Pacific-Farallon mid-ocean ridge (MOR) to above the Farallon slab (−120° to −90°), similar to that inferred in previous studies (Zhou et al., 2018). This Poiseuille-type flow is induced by the downwelling Farallon slab to the east, which created a low-pressure zone above it (Fig. 7). Since both models largely reproduce the major slab structure and mantle flow, we expect that they should have similar slab evolution over time, given their common surface plate kinematics. Since subduction started, both models are featured by a low-pressure zone above the Farallon slab (Fig. 7). The low pressure in the mantle wedge leads to the trench-ward flow beneath North America. Both models, due to the progressively increasing pressure gradient across the sinking slab, reproduced the Late-Cretaceous flat Farallon slab (Fig. 7c,g), which is consistent with the inference from previous studies (Jones, 2012; Liu et al., 2008; Saleeby, 2003). After detachment of the flat Farallon slab from the above lithosphere, the dynamic pressure gradient induced a strong eastward flow from the Pacific mantle to that inland, a similar phenomenon observed below East Asia after subduction of the Izanagi-Pacific MOR (Peng et al., 2021a).

On the other hand, there are some notable differences in the large-scale mantle flow. Along the east-west cross section, prior to the Cenozoic there was a fast westward lower mantle flow in the global model (Fig. 7a) but not in the regional one (Fig. 7e). This westward component of mantle flow in the global model gets weaker with time (Fig. 7), but gradually turns more southward toward the present (Fig. 6). In the regional model, however, the lower-mantle flow is almost negligible at all times (Figs. 6, 7), consistent with the effect of the rigid side walls. Consequently, the global model has the Farallon slab subducted to a location slightly southwest of that in the regional case, with the former more consistent with tomography. It is anticipated that the mismatch in the regional model cannot be solved by varying the model domain which will unlikely generate the southwestward mantle flow required to match tomography. This reinforces our finding that regional models cannot resolve large-scale mantle flow as usually occurs in global models.

The match of the regional model result to tomography for North America is slightly worse than for Tonga. Assuming the regional results for North America and Tonga are both acceptable, we further analyze the reason for their suitability. The Tonga subduction history is short (from 50 *Ma*), but that for the eastward subduction below North America covers almost the entire model duration (from 190 *Ma*).

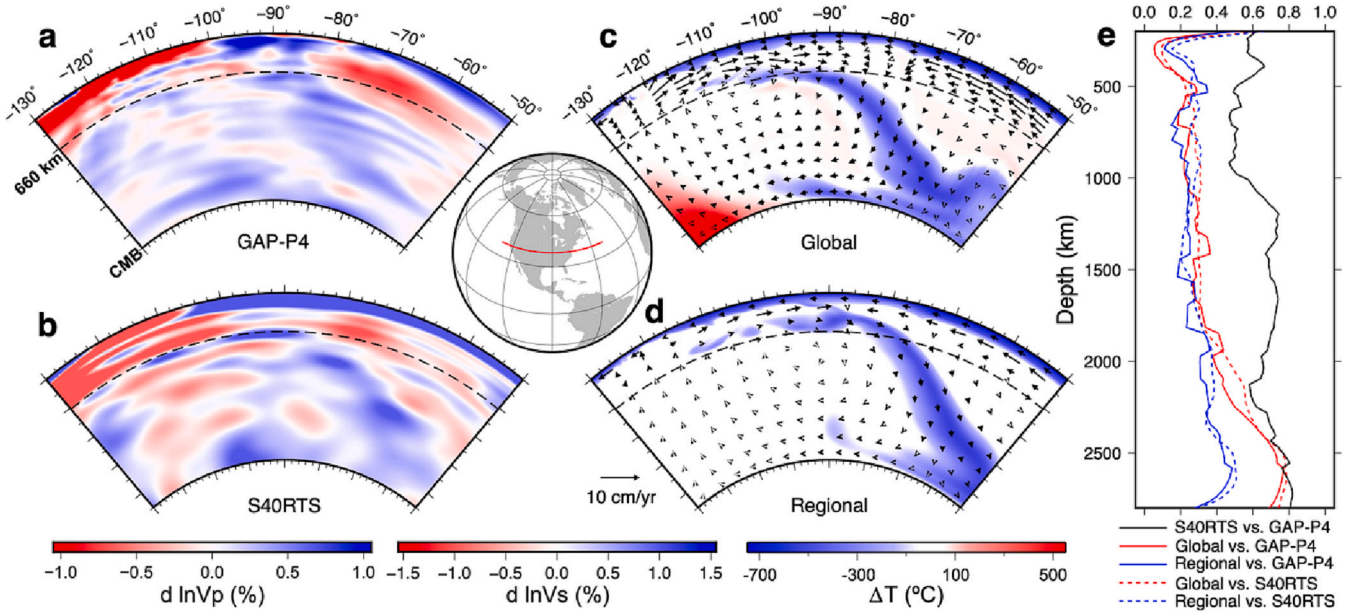

Fig. 5. The Farallon slab beneath North America in tomography, the global model and regional model. The panel in the center marks the cross-section of 38°N with the red line. (a,b) Seismic wave velocity anomalies in GAP-P4 and S40RTS, respectively. (c,d) Model temperature anomalies and velocities in the global model and regional model, respectively. (e) Sensitivities of the global (red curves) and regional (blue curves) models against GAP-P4 and S40RTS. The sensitivity of S40RTS against GAP-P4 is also shown (black curve) as a reference. The seismic velocity anomalies for the same cross-section are shown for MIT-P08, UU-P07 and SEMUCB-WM1 in Fig. S2, along with the sensitivity and accuracy. (For interpretation of the references to colour in this figure legend, the reader is referred to the web version of this article.)

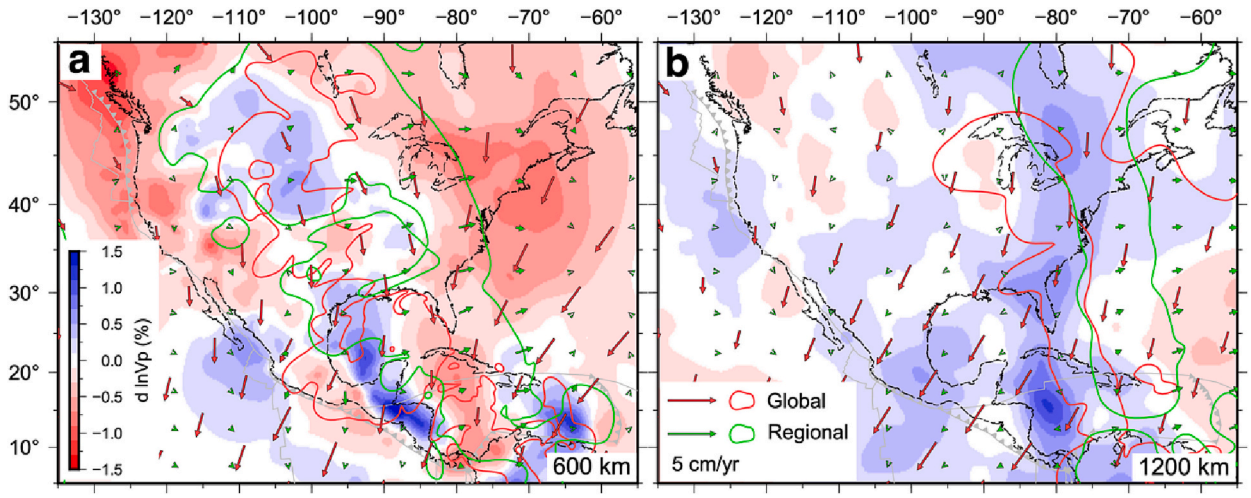

Fig. 6. The mantle convection models compared with GAP—P4. The background colour shows P wave velocity anomalies at 600 km (a) and 1200 km (b). The contours (−100 °C) show cold temperature anomalies in the global model (red) and regional model (green). The arrows show mantle velocities in the global (red) and regional (green) models. (For interpretation of the references to colour in this figure legend, the reader is referred to the web version of this article.)

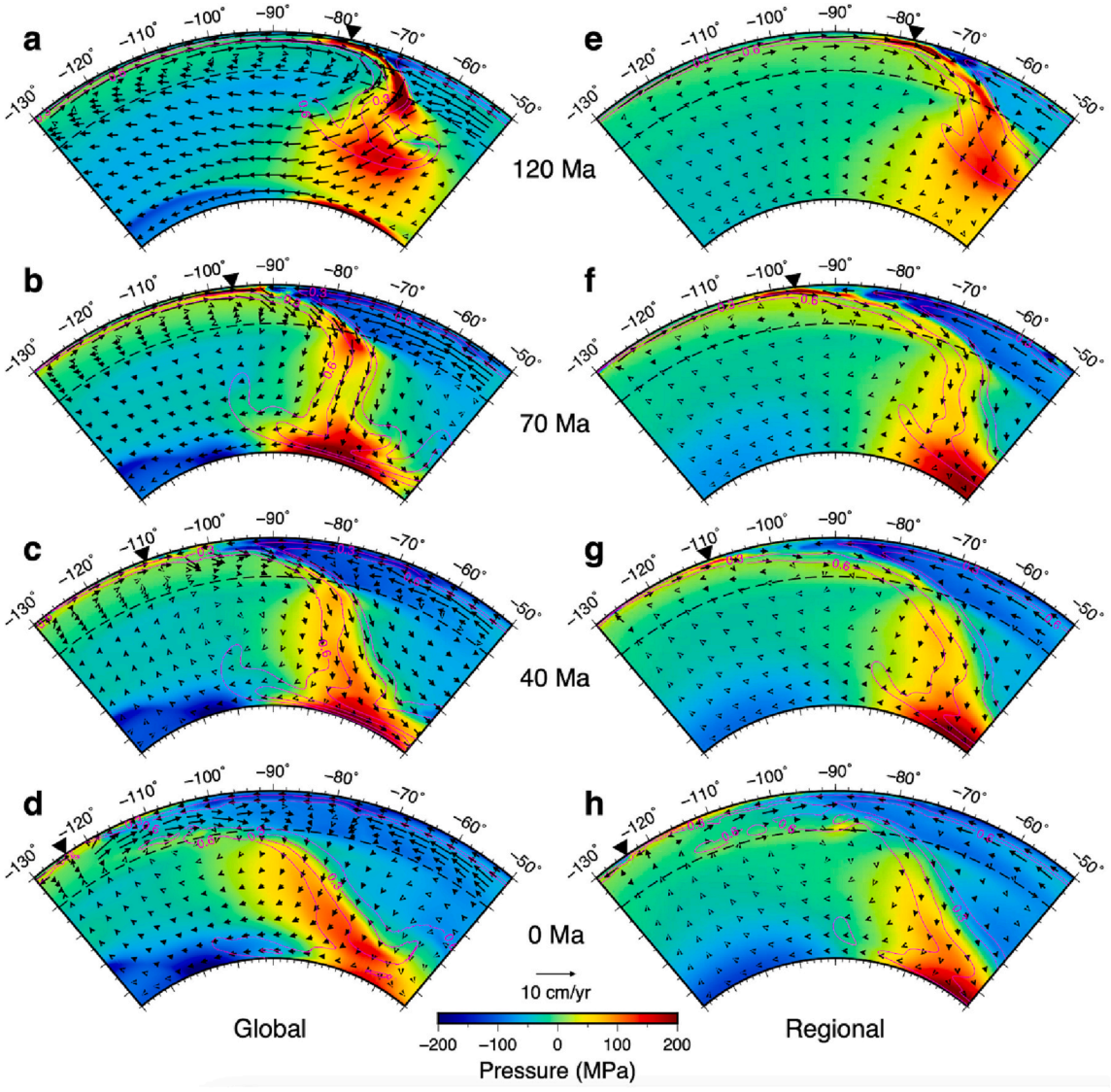

Fig. 7. The evolution of Farallon slab, dynamic pressure, and velocity field in the models beneath North America along 38°N. (a-d) Global model evolution with time snapshots at 120 *Ma*, 70 *Ma*, 40 *Ma* and 0 *Ma*, respectively. (e-h) The same as (a-d) but for the regional model.

Although the subduction history differs, both regions have considerable trench retreat (Fig. 1). North America moved over 60° westward from 200 *Ma* (Müller et al., 2016). The upper-mantle flow is largely Poiseuille-type, driven by dynamic pressure from the sinking Mesozoic slabs underneath (Fig. 7). The direction of the Poiseuille flow is the same as the overriding plate movement, so that the difference between the global and regional models is partially compensated because of the imposed surface velocity. Consequently, both the global and regional models in North America produced a flat Farallon slab in the Late Cretaceous to early Cenozoic, and also generated similar slab geometries at the present. Part of the differences between the two models, such as the depth of the slabs, might be mitigated by adjusting mantle dynamic parameters (e.g., mantle viscosity), which is still not well constrained. We therefore suggest that regional models may be suitable for simulating North American subduction in practice.

3.3. South America

Along the west coast of South America, subduction of the Farallon/Nazca plate started at least in the Mesozoic (Müller et al., 2016). The subduction has contributed to the formation of a series of tectonic features including the Andes (Hu et al., 2021; Schellart et al., 2007) and the abnormal distribution of volcanism and earthquakes (Hu and Liu, 2016; Jordán et al., 1983). With a width of about 7000 km, the trench is the longest at the present. The South American subduction zone displays strong along-trench variations in slab dip angle. The subducting Nazca slab has multiple segments of flat slabs (Espurt et al., 2008; Gutscher et al., 2000), including the Bucaramanga, Peruvian and central Chile flat slabs, intervened by normal dipping slab segments. Since these flat slabs are sensitive to local slab buoyancy features (Hu et al., 2016; Jordán et al., 1983) that are not incorporated in our global model, we focus on the large-scale along-trench variation of slab structure. In particular, we first examine a cross-section showing a proposed stagnant slab near 660 km depth (Fig. 8a,b). The configuration of this stagnated portion of the Nazca slab (Contenti et al., 2012; Portner et al., 2020) seems less well resolved (Fig. 8a,b) than the stagnant slabs in East Asia and Tonga. Multiple tomography inversions show accumulated fast seismic anomalies near the 660 km discontinuity at the southern part of the South American trench, although with the resolving power varying from P-wave (e.g., UU-P07, Fig. 8) and S-wave models (e.g., SEMUCB-WM1, Fig. S3).

The Nazca slab in the global model is deformed and stagnant at the top of the lower mantle (Fig. 8c), as fits tomography very well (Fig. 8a, c). In contrast, the slab in the regional model appears much longer and deeply penetrates the lower mantle (Fig. 8d). Given that the two models utilize the same plate kinematic history at the surface, the apparently shorter slab in the global model is mainly because it is folded and horizontally compressed by lateral mantle flow. The folding of Nazca slab near 660 km is also proposed in previous studies (e.g., Faccenna et al., 2017). In map views, the slabs predicted by the global model also fit tomography well at both the MTZ (Fig. 9a) and lower mantle (Fig. 9b), but the regional model has obvious mismatches at these depths. Besides the Nazca slab, there are other cold anomalies at lowermost mantle depth in the global result (Fig. 8c), which is absent in the regional case (Fig. 8d). As we recently showed (Peng and Liu, 2022), these deep cold anomalies beneath the Nazca plate represent the Mesozoic Farallon slab which migrated a long distance from North America southward following the large-scale mantle flow (Figs. 6, 9), a feature clearly missing in the regional model. Collectively, the sensitivities of the global model against tomography results are better than the regional one consistently for mantle deeper than 500 km (Fig. 8e), because of the correctly predicted slab positions and geometries.

The different slab geometries from the two models could be explained using the patterns of dynamic pressure and mantle flow (Figs. 8c,d, 10). Both dynamic pressure and mantle flow in the regional model are intuitive in that a natural supra-slab return flow formed within the lower-pressure mantle wedge. In contrast, the global model, for most of the geological past, had a higher pressure within the mantle wedge than below the slab, as is counter-intuitive for a single-slab environment. Physically, this reversed pressure structure is due to the downward drag of the previously subducted Farallon slab that migrated southward and arrived beneath the subducting Nazca slab after 40 *Ma*

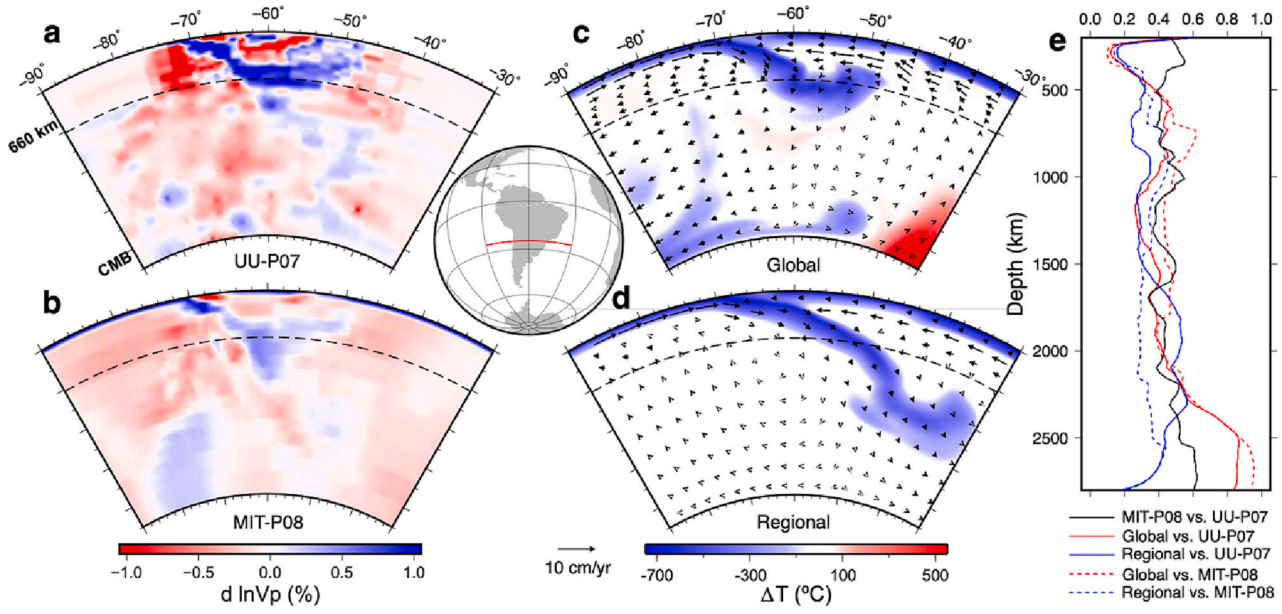

Fig. 8. The Nazca slab beneath South America in tomography, the global model and the regional model. The panel in the center marks the cross-section of 25°S with the red line. (a,b) Seismic wave velocity anomalies in UU-P07 and MIT-P08, respectively. (c,d) Temperature anomalies and velocities in the global model and regional model, respectively. (e) Sensitivities of the global (red curves) and regional (blue curves) models against UU-P07 and MIT-P08. The sensitivity of MIT-P08 against UU-P07 is also shown (black curve) as a reference. The seismic velocity anomalies for the same cross-section are shown for GAP—P4, S40RTS and SEMUCB-WM1 in Fig. S3, along with the sensitivity and accuracy. (For interpretation of the references to colour in this figure legend, the reader is referred to the web version of this article.)

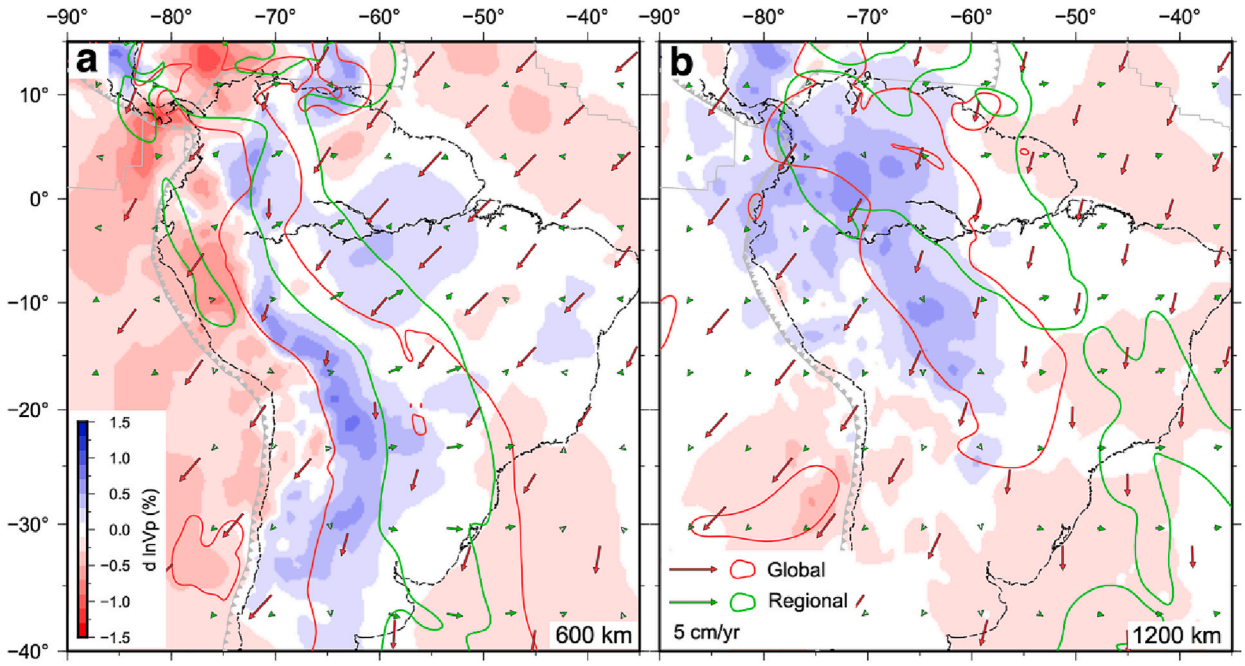

Fig. 9. The mantle convection models compared with MIT-P08. The background colour shows P wave velocity anomalies at 600 km (a) and 1200 km (b). The contours (−100 °C) show low temperature anomalies in the global model (brown) and regional model (green). The arrows show the mantle convection velocities in the global model (brown) and regional model (green). (For interpretation of the references to colour in this figure legend, the reader is referred to the web version of this article.)

(Fig. 10b,c). The arrival of the deep Farallon slab and the accompanying 3D mantle flow could be a reason why the Nazca slab stopped sinking after 40 *Ma* and started to pile up at the base of the upper mantle. The regional model does not simulate the Farallon subduction, so the only slab, the Nazca, sunk into the lower mantle and kept going deeper (Fig. 10e,f). Another possible reason for the stagnant slab in the global model might be the presence of the African LLSVP beneath the slab front (Fig. 8c). However, since this LLSVP is not generating any upwelling motion in the mantle (Fig. 10b,c), similar to the limited effect of the Pacific LLSVP beneath Tonga on shaping the slab structure, we suggest that the southward approaching deep Farallon slab is the dominant reason for the different mantle dynamics and slab geometries in these two models.

3.4. East Asia

East Asia is a tectonically active area with a complex subduction history since the early Mesozoic. The southern side experienced the subduction of the Tethyan slabs and the India-Eurasia collision which eventually created the Tibetan Plateau (England and Houseman, 1986). On the eastern side, the long-last subduction of the Izanagi slab, Pacific slab and Philippine slab are thought to be the dominant reason for major tectonic features including the destruction of the North China Craton (NCC), the migration of volcanisms, the opening of back arc basins, the topography distribution and lithospheric structure (Li et al., 2014; Li, 2000; Liu et al., 2021a; Liu et al., 2021b; Peng et al., 2021b; Wu et al., 2019; Yin, 2010). The present-day slabs beneath East Asia are characterized by the >1500 km long stagnant part in the MTZ, commonly recognized in numerous tomographic images (Fukao et al., 1992; Huang and Zhao, 2006; Li et al., 2008). The global model reproduced the stagnant Pacific slab consistent with that in the tomographic images (Fig. 11a-c) whose upper-mantle slab structures are most consistent with region studies (e.g., Huang and Zhao, 2006). However, in the regional model, the Pacific slab clearly penetrates the 660 km discontinuity with no stagnation (Fig. 11d). Relative to the upper mantle structure, the distribution of lower mantle slabs is more uncertain among different tomographic results (Fig. 11a,b). Quantitatively, the global model also fits the lower-mantle tomography better than the regional models, except for the mid-mantle (Fig. 11e). The tomography reveals more lower-mantle slabs within the central-western portions of the profile than in the easternmost portion, as support the global model prediction. In the mid-mantle, the global model predicts a weak slab associated with young seafloors around the Izanagi-Pacific mid-ocean ridge, while tomography suggests multiple pieces of fast anomalies. Volumetrically, this explains why the regional model matches tomography better in this depth range, although the modeled slab location is off.

Except for the better resolved present-day stagnant slab beneath East Asia and the higher sensitivities against tomography in the global models (Figs. 11, S4, Table S1), there are other reasons for us to suggest that the global model is more suitable in modeling the subduction process in East Asia. First, the lower mantle slabs in the regional model are systematically eastward shifted. Second, the global model predicts a continental scale flat Izanagi slab in the Late Cretaceous that matches multiple lines of geologic data (Liu et al., 2021b; Peng et al., 2021b), while the regional model fails to produce this feature (Fig. 12). This early flat slab sank to the lower mantle at the present, with a location clearly more to the west compared to the regional result. Third, the failure of the regional model in generating the present stagnant upper-mantle slabs also explains its eastward-shifted lower-mantle slabs, given the apparent spatial connection between these slabs.

To further understand why the regional model fails to reproduce the stagnant slabs and the correct positions of the lower mantle slabs as the global model does, we investigate their temporal evolution (Fig. 12). The global model consistently maintains a prominent low-pressure mantle wedge above the slab, a feature that is nearly absent in the regional model. As revealed previously (Peng et al., 2021a, 2021b), this strong gradient in dynamic pressure across the slab is a result of multi-slab interaction, where the orthogonally oriented Tethyan and Izanagi slabs enhanced the depressurization of their overlapping mantle wedge beneath East Asia. This also represents the key reason for the formation of both the flat Izanagi slab during the Late Cretaceous (Fig. 12a,b) and the stagnant slabs at the present-day (Fig. 12c,d). In the regional model,

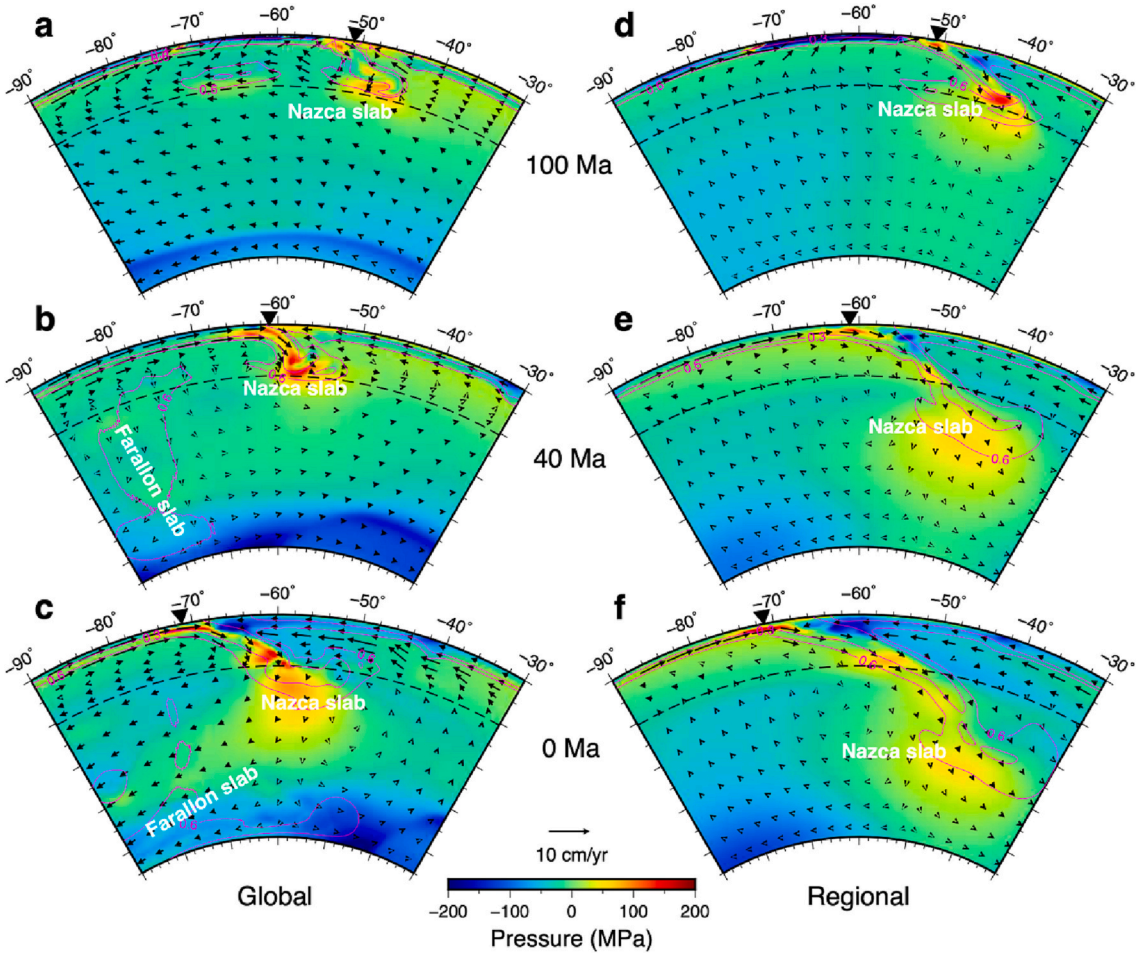

Fig. 10. The evolution of Nazca slab, dynamic pressure, and velocity field in the models beneath South America along 25°S. (a-c) Global model evolution with time snapshots at 100 *Ma*, 40 *Ma* and 0 *Ma*, respectively. (d-f) The same as (a-c) but for the regional model. Specifically, in the global model, the subducted Farallon slab underlies the subducting Nazca plate since 40 *Ma* (b-c).

the Izanagi slab sank more vertically during the Late Cretaceous (Fig. 12e-f), where the lack of strong dynamic suction force fails to form a flat slab.

We suggest this difference in model behavior is due to the free-slip side walls in the regional case. The global model captures multiple subduction systems, as allow remote slab interaction and the occurrence of large scale mantle flow (e.g., westward lower mantle flow in Fig. 12a, b,d facilitated by other large-scale mantle downwellings like the Farallon and Tethyan subduction systems (Fig. 12)). In contrast, the artificial non-permeable side boundaries in the regional model render this impossible (Fig. 12e,f). Such a model discrepancy cannot be reconciled with different mantle viscosity or density parameterizations. As a main factor forming the Cenozoic mantle wind that shapes the stagnant slabs, the landward position of the former Izanagi slab inside the lower mantle is important. In the global model, the Izanagi slab travels >2000 km westward prior to 70 Ma, whose subsequent sinking helped to generate the westward flow beneath East Asia (and eastward flow west of 110°E) (Fig. 12c,d). In the regional model, the slab is subducting more steeply and largely beneath the trench, thus creating mostly eastward flow beneath East Asia (Fig. 12g,h). Consequently, this results in a sub-vertical slab pile below the subduction zone, as expected for a single-slab system.

Next, we use 2D regional models to test if increasing the model domain helps to reproduce the large-scale mantle flow and improve the model results. We increase the span of longitude from 60° to 180° from 2D models 1 to 4. Besides the different model domains, the distance of the present-day trench from the eastern (western) model boundary in the 2D models also varies, being about 1400 km (5300 km), 1400 km (9800 km), 3600 km (12,000 km), and 8000 km (12,000 km), respectively. It turns out that none of these models can correctly reproduce the stagnant Pacific slab at the present (Fig. 13). This indicates that neither the model domain nor the trench location within the model domain help generating the correct slab structures. On the other hand, the average depth of lower-mantle slabs is getting deeper from model 1 to model 4, as is because the wider models have more space for the subducted slabs to spread laterally and to generate return flow that alleviates vertical resistance to slab sinking. For example, there is a strong trench-ward asthenospheric return flow induced by the slab sinking in models 2–4 (Fig. 13b-d). This flow, however, is very weak in model 1 (Fig. 13a), because the left boundary which is close to the slab impedes its formation.

The sensitivity against GAP-P4 of these 2D models between 100°E and 160°E in the whole-mantle depth is 0.70, 0.56, 0.51 and 0.51, respectively. The sensitivity calculated in the same region for the global 3D model and regional 3D one is 0.71 and 0.66 respectively. Among these models, the global one performs significantly better than others (Figs. 11, 13). The results of the 2D models and the 3D regional model, although with different model dimensions, are not too different. Therefore, we confirm that the global model is preferred for modeling subduction beneath East Asia. The large-scale westward mantle flow required to form the observed location of the present lower-mantle Izanagi slab and the formation of upper-mantle stagnant slabs cannot be generated within regional models, irrespective of the adopted model domain.

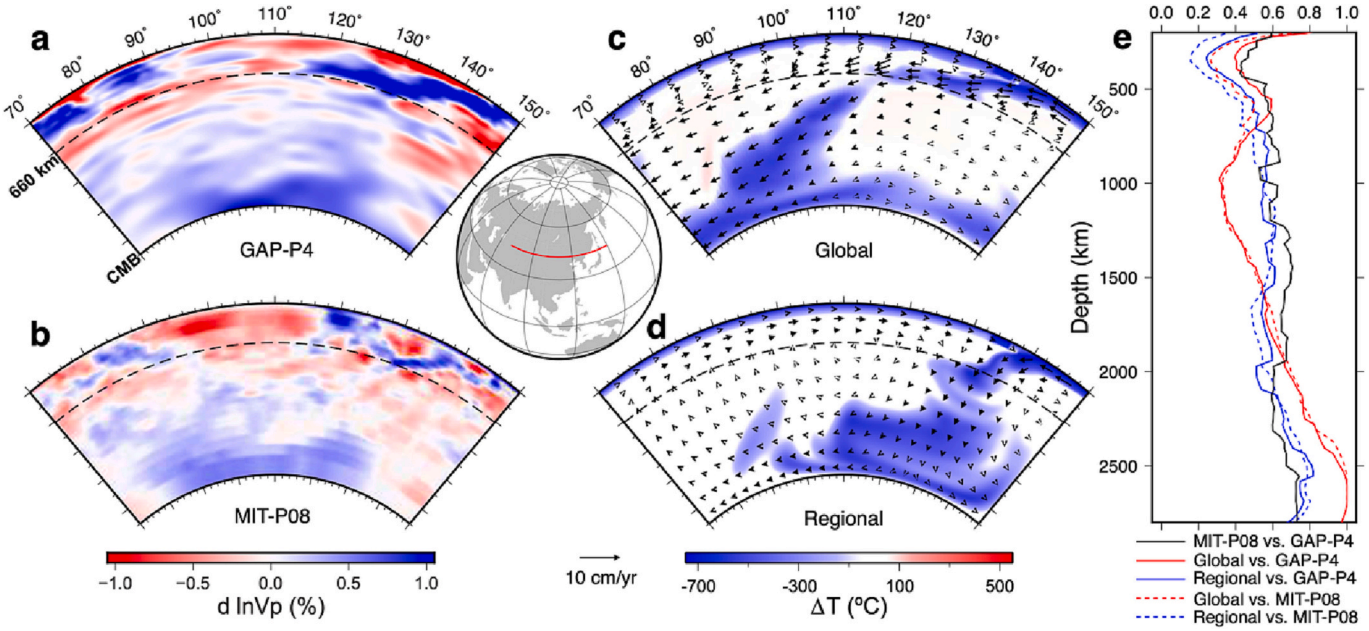

Fig. 11. Pacific slabs beneath East Asia in tomography, the global model and the regional model. The panel in the center marks the cross-section of 43°N as the red line. (a,b) Seismic velocity anomalies in GAP-P4 and MIT-P08, respectively. (c,d) Temperature anomalies and mantle flow in the global and regional model, respectively. The dashed lines show the 660 km discontinuity. (e) Sensitivities of the global (red curves) and regional (blue curves) models against GAP-P4 and MIT-P08. The sensitivity of MIT-P08 against GAP-P4 is also shown (black curve) as a reference. The seismic velocity anomalies for the same cross-section are shown for UU-P07, S40RTS and SEMUCB-WM1 in Fig. S4, along with the sensitivity and accuracy. (For interpretation of the references to colour in this figure legend, the reader is referred to the web version of this article.)

4. Discussion

By comparing the results of the 3D global model, 3D regional models and 2D regional models, we find that 3D regional models successfully reproduced the major features of mantle flow and slab structures for subduction zones in Fiji-Tonga and North America. On the other hand, for South America and East Asia, the global model is significantly better than the regional ones in generating the correct slab geometries. We propose that the non-penetrative side walls in the regional models and the pattern of surface plate motion determine the overall suitability of regional models in replicating real Earth processes. However, more factors remain to be discussed about the influences of boundary conditions, model parameters and other possible ways to improve the regional models. Below, we discuss the relative lengths of subducted slabs and motion of the overriding plate, as well as different types of side boundary conditions in regional models.

4.1. The influence of side walls and far-field effects

In the previous sections, we have shown that the boundary conditions for the regional models are critical for their results. Their effects on modeled mantle flow and slab evolution in global and regional models are summarized below (Fig. 14). Fast movements of the overriding plate could strongly modulate the underlying mantle by generating a dominant Couette-type flow pattern (Fig. 14a). Similarly, the subducting plate also controls the Couette flow beneath it. In this case, the overriding plates dominant the shallow mantle flow, a scenario that applies to both regional and global models. In the lower mantle, the mantle flow pattern tends to be a simple return flow due to the surface plate motion. There is a difference that the global model allows influx and outflux across any hypothetic vertical wall, which is not the case in the regional model. However, this difference has limited influence on the slab as long as it remains far from the side walls. As a result, the slab is under similar background flow, thus similar sinking direction (Fig. 14a). This condition applies to the Tonga and North America, as well as other subduction zones with fast moving overriding plate.

In the case of slow-moving upper plate, the flow underneath is less affected by the plate motion above and more by internal mantle processes, where the flow could form a Poiseuille-type with a faster-than-surface velocity driven by the suction of the actively sinking upper-mantle slab (Fig. 14b). Because of the Couette flow beneath the subducting plate, the global model could also produce a large-scale landward flow. In the regional one, on the other hand, the deep flows beneath the subducting and overriding plates tend to form separate convection cycles due to the impermeable side walls (Fig. 14b). Consequently, the slab in the global model has more landward motion than in the regional one, and eventually they will have different positions and geometries. The subduction zones on the west of South America and east of Asia are close to this scenario. We expect that a global model works better than a regional one for other subduction systems with a similar setting.

Other far-field effects that influence the slab evolution include slabs from beyond the study region (Fig. 14a) and LLSVPs (Fig. 14b). How these other slabs and LLSVPs change the mantle flow and the slab evolution at investigation varies with their positions and physical properties (Yang et al., 2019). For regions with long and complex subduction history, the former factor may be more important, such as East Asia. For subduction zones close to LLSVPs, we may see more impacts from these hot materials.

4.2. The ratio of overriding-to-subducting plate movements

For the circum-Pacific subduction zones, we estimate the distances over which the upper plate and the subducting plate traveled based on the plate reconstruction (Müller et al., 2016), following three steps. First, we measure the average along-trench velocity of an oceanic plate (i.e., subduction rate averaged along the trench) in million-year increment. Second, we calculate the total distance the oceanic plate traveled (subducted) since 200 *Ma*. Third, we select a stable craton (except for Tonga) above each of the subduction zone to calculate the overriding

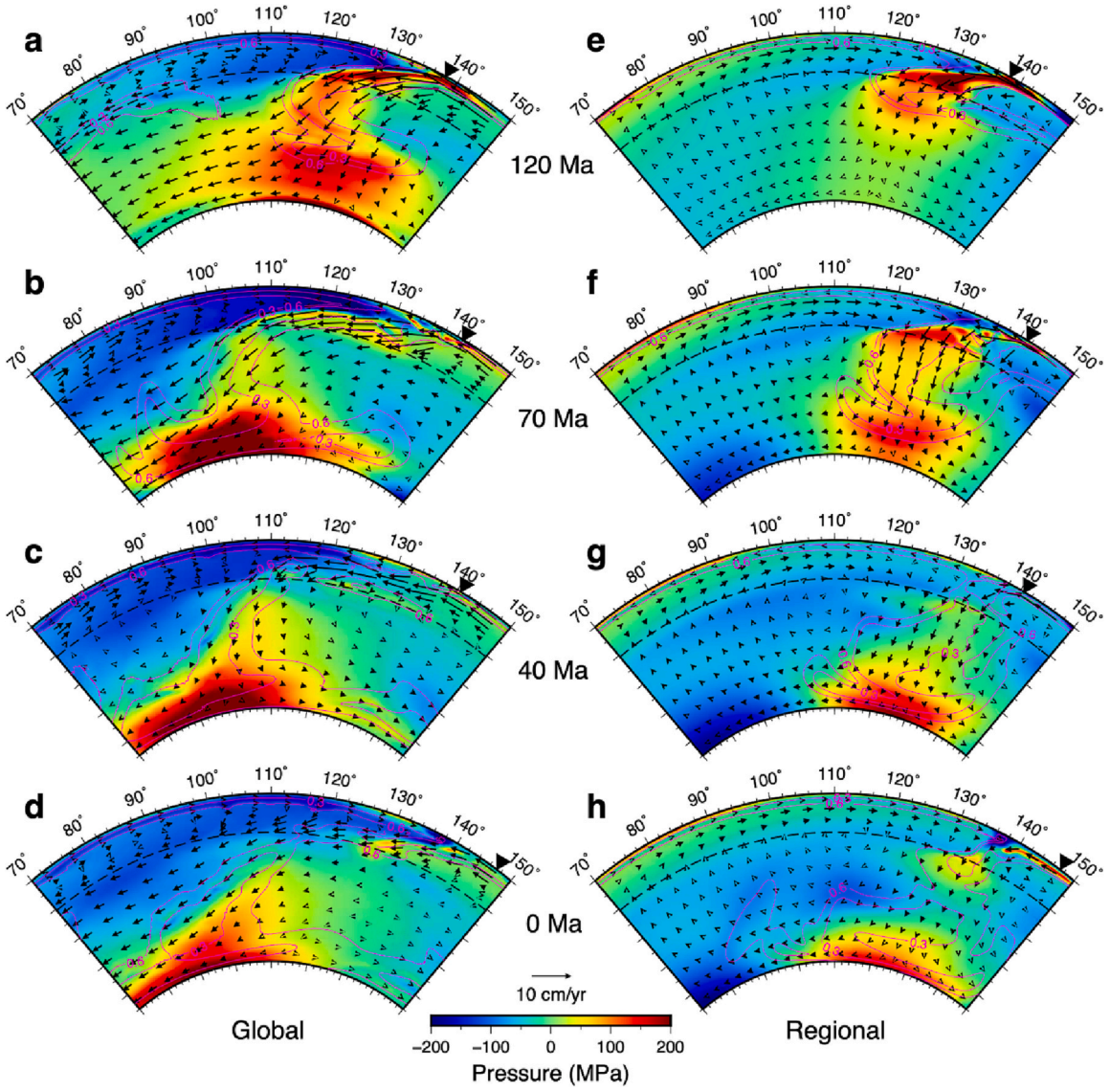

Fig. 12. The evolution of slabs, dynamic pressure, and velocity field beneath East Asia. (a-d) Global model evolution with time snapshots at 120 *Ma*, 70 *Ma*, 40 *Ma* and 0 *Ma*, respectively. (e-h) The same as (a-d) but for the 3D regional model. The cross-sections are along 43°N. The magenta contours representing −100 °C and −400 °C temperature anomalies show the slab structure. (For interpretation of the references to colour in this figure legend, the reader is referred to the web version of this article.)

plate motion. For East Asia, North America and South America, the utilized cratons are North China Craton, Slave Craton and Amazonia Craton, respectively. The cumulative plate movements are the average distance these cratons migrated since 200 *Ma*. For the Tonga subduction zone, there is no craton suitable to represent the motion of the overriding plate, due to the dominant ocean-ocean subduction and strong back-arc extension during the Cenozoic. Therefore, we simply take the present-day trench retreat speed and subduction rate of Pacific Plate near the trenches as proxies for the movements of the overriding and subducting plates.

Since 200 *Ma*, the NCC migrated ~2470 km southwest ward, while the Izanagi/Pacific subducted ~19,700 km. This corresponds to a ratio of overriding plate motion (OR) to subduction (SD) of OR/SD = 13.7%. North America migrated northwest by ~5240 km and the subducted slab length along its west coast is 12,700 km, leading to OR/SD = 49.0%. South America moved ~2840 km northwest with the subducted slab length being ~11,500 km, so OR/SD = 24.7%. For Tonga, the trench retreat rate varies from 3 cm/yr to 16 cm/yr along the Trench (Schellart et al., 2007), and the subduction rate varies from 7 cm/yr to 8 cm/yr. Based on these data, the present-day OR/SD varies from 42.9% to 200%. Since the subduction zones discussed in this study are facing mainly eastward or westward, we also calculated the ratios along the *E*-W direction. The corresponding OR/SD ratios are 5.9%, 48.3%, and 24.2% for East Asia, North America, and South America, respectively. The value in East Asia is notably smaller than that estimated above, since its overriding plate motion is mainly southward.

Therefore, East Asia represents the case where the overriding motion is dominated by the subducting motion. This allows the far-field effects to play an important role in affecting the local mantle flow and slab geometry. In contrast, North America and Tonga have comparable overriding and subducting motions, where the retreating trench following the upper plate can significantly influence the local mantle flow and thus geometry of the subducting slab. As a result, the regional models, and the global model, which assimilate the same plate motion, result in more similar slab structures compared to that in East Asia. South America stands as an intermediate case between these two end-member scenarios.

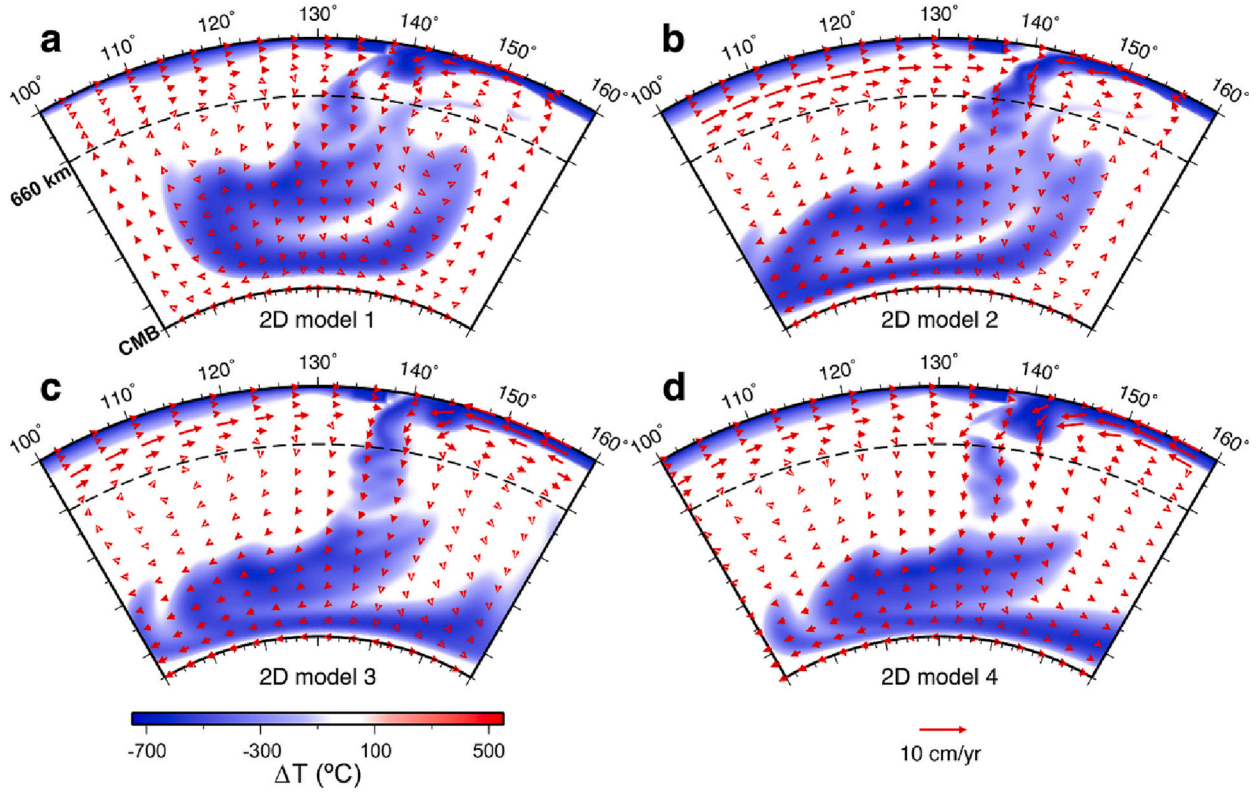

Fig. 13. The slab structure and velocity field of 2D models. Since model 1 only covers 100°E to 160°E, all models are plotted for the same region.

4.3. Types of boundary conditions and their effects

In this study, all the regional 3D models and 2D models have free-slip boundaries on the side walls. A free-slip boundary allows no velocity normal to the side walls but does not constrain motion in other directions. This is also referred to as a reflecting boundary. There are other types of boundary conditions for velocity on the side walls that we have not tested, including no-slip, prescribed velocity, periodical and hybrid boundary conditions. Different from free-slip, no-slip boundary condition forces all velocity components to be zero on the side walls. A prescribed velocity condition is similar as no-slip but could allow a non-zero normal velocity instead. On the side walls, such prescribed velocities mimic influx and outflux of material through the boundaries, usually following the conservation of mass within the model domain. A periodical boundary assumes that the side walls allow influx and outflux, but their patterns are cyclic: materials flow out of the left boundary and re-enter through the right boundary. Different boundary conditions can also be combined to form a hybrid one.

The key disadvantage of regional models with impermeable side walls is the lack of large-scale mantle flow. No-slip boundaries prohibit flow through the side walls just the same as the free-slip case. Thus, regional models with no-slip walls cannot create the large-scale mantle flow. Similarly, it is also impossible to account for the effect of slabs from other subduction zones as the model evolves. Previous studies showed that models with free-slip boundary condition on the side walls generally have large slab dip angle, while a periodical boundary helps to create naturally dipping slabs (Gurnis and Hager, 1988; Han and Gurnis, 1999; Zhong and Gurnis, 1995). A periodical boundary may be able to generate strong lower mantle flow, but it may conflict with observed surface velocity, the lithospheric thermal and compositional profiles that are not periodic in nature.

Prescribing a non-zero side velocity, however, is a good candidate for improving regional models. By implementing boundary influx and outflux, there will be a net velocity throughout the model domain which mimics the large-scale mantle flow. A potential way forward is to extract the velocities at locations of the side walls of the regional model from the global model and apply these velocities as the influx/outflux velocities on the walls. This is similar as earlier efforts with a high-resolution regional model embedded in a forward global model (Tan et al., 2006) or with mantle flow velocities back-advected from density based on tomographic results (Chertova et al., 2018), but will be more flexible and computationally efficient. It remains unclear how this approach could accommodate other far-field effects which naturally arising in a global model, like the LLSVPs and other slabs. An application of this method is warranted for future studies.

4.4. Influence of model parameters on the results

The models presented here assume the Boussinesq approximation. The mantle temperature is simplified with no adiabatic temperature increase. These assumptions may lead to colder and thicker slabs than models assuming a compressible mantle (Flament, 2019). To analyze the influences of the potentially thickened slabs, we calculated the sensitivity of model against tomography by increasing the thresholds of anomalies (Table S2). The temperature threshold for slabs is 7% colder than the ambient mantle. The thresholds for P wave and S wave seismic anomalies are 0.2% and 0.3%, respectively. This calculation excluded the anomalies which have similar values as the ambient mantle, thus more restricted to the slabs. As a result, we see increased values of sensitivity (Table S2 vs. Table S1). Additionally, whether temperature alone can explain the seismic velocity remains debated (Davies et al., 2012; Schuberth and Bunge, 2009). It would be more appropriate to convert the model thermal anomalies into seismic velocity perturbations in future studies.

Another simplification is that the regional models have no initial thermal-chemical pile for modeling LLSVPs. It may be one reason why the global model has higher sensitivities against tomography than the regional models in the deep mantle. Moreover, the physical properties

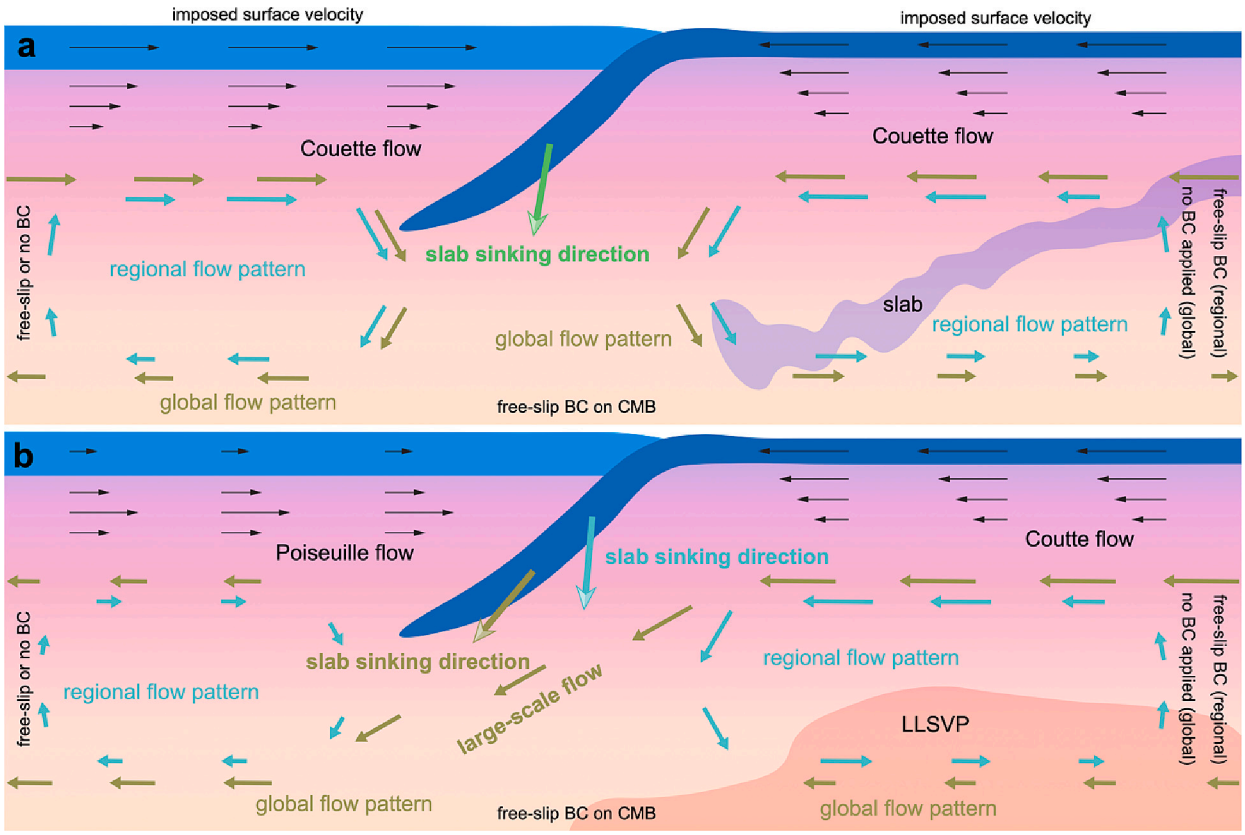

Fig. 14. A sketch of mantle flow in global and regional models with different upper-plate motions. (a) With fast trench retreat, the rapid motion of the overriding plate induces a Couette flow beneath it, similar to that below the subducting plate. In both global and regional models, the lower-mantle flows beneath these plates are likely a simple return flow from the surface motion. (b) When the velocity of the overriding plate is small, the mantle flow underneath could become a Poiseuille-type, driven by slab suction. The global model could also produce a large-scale landward flow driven by far-field effects. In the regional model, the return flow at depths is limited in amplitude due to the impermeable side walls. The presence of other slabs (a) and/or LLSVPs (b) may also influence the evolution of the subducting slab. BC - boundary condition.

(e.g., temperature, density and viscosity) of the LLSVPs are still uncertain (Flament, 2019; Hassan et al., 2016; Lau et al., 2017). Increasing the density and viscosity of the LLSVPs tends to spread them out laterally (Hassan et al., 2016), but their large-scale evolution remains similar due to the dominant effects of slabs (McNamara and Zhong, 2004). Varying the initial pile thickness (to smaller than ~250 km) may change the heights of LLSVPs, but there will be two separate LLSVPs generated whose shapes remain close to tomographic results (McNamara and Zhong, 2004). The influence of the LLSVP parameters (when varying in a reasonable range) on slabs in shallower mantle is likely small since the LLSVPs are mainly passively driven by subducted slabs (McNamara and Zhong, 2004; Peng et al., 2021b). Till today we still know little about materials in deep mantle and the corresponding model parameters have large uncertainties. The model (the global model in this study) which matches observations the best is supposed to best represent the real Earth. In general, stronger temperature and density contrasts enhance the convection vigor and likely lead to deeper slabs. Weaker background viscosity has a similar function. However, changing these model parameters mostly affect vertical evolution, but cannot amend the identified effects of far-field dynamics in regionals models that cause changes more on the lateral direction.

5. Conclusion

In this study we run data-assimilation subduction models and compare the results of a global model with regional models for all the major circum-Pacific subduction zones. The stagnant Tonga slab is reproduced by both the global model and regional model. We suggested two reasons for the validity of the regional model. First, the lower mantle beneath the Tonga subduction zone is a deprived of slabs because of the short subduction history. Thus, the subduction of Tonga slab is not influenced by the buoyancy structures from prior or other subduction zones. Second, the fast retreat of Tonga trench may be the dominant mechanism for the formation of the stagnant slab and both models have the trench motion incorporated from plate reconstruction. North America is a region where the result of the regional model is not as good as the global one, but still reproduced the major slab features. Like Fiji-Tonga, the subduction zone along the western coast of North America also has fast trench retreat. North American plate moved over 60° westward since the Jurassic. This plate motion played an important role on the local-scale mantle flow and dipping of the Farallon slab in the lower mantle. For South America, the global model matches tomographic results much better than the regional model, likely because of a segment of Farallon slab beneath the subducting Nazca slab. This slab segment traveled from beneath North America to South America following the large-scale mantle flow which is missing in the regional model because of the impenetrable side walls. For East Asia, the slab structures in the global model match tomographic results but those in the regional models do not. We find that the large-scale flow in the lower mantle naturally produced by the global model is important for the continuous westward migration of the Izanagi slab. In turn, the westward shifted Izanagi slab dominated the formation of regional mantle wind which ultimately controlled the stagnation the slabs. The missing large-scale lower mantle flow in the regional models cannot be established by increasing the model domain. Based on the above analyses, we make the following suggestions for future development of subduction

models with data-assimilation.

(1) Global models are generally better than regional ones, because they can resolve large-scale mantle flow, dynamic pressure, and possible interactions among slabs and LLSVPs.

(2) In regions with complex mantle structures like East Asia and South America, regional models should be designed with caution to overcome the problems caused by the side walls.

(3) Regional models can be safely applied to regions like North America and Tonga, where the overriding plate moves fast to play an important role on subduction dynamics.

Declaration of Competing Interest

The authors declare that they have no known competing financial interests or personal relationships that could have appeared to influence the work reported in this paper.

Data availability

The data sources are included in the acknowledgement.

Acknowledgements

This work is supported by NSF grant EAR1554554. D. Peng acknowledge the support of Green Postdoctoral Scholarship. We thank the editors Gillian Foulger and Dietmar Müller, reviewer Nicolas Flament and an anonymous reviewer for their comments and suggestions which greatly helped to improve this work. We thank D. Stegman for valuable discussions. We acknowledge the Texas Advanced Computing Center (TACC) for providing Frontera allocation. Most figures are prepared with GMT (https://www.generic-mapping-tools.org/) and Paraview (https://www.paraview.org/). Surface velocity and plate boundary files are exported using Gplates (https://www.gplates.org/). The original version of CitcomS is available at www.geodynamics.org/cig/software/citcoms/. The P-wave tomography model UU-P07 is available at https://www.atlas-of-the-underworld.org/uu-p07-model/. GAP-P4 is available at http://d-earth.jamstec.go.jp/GAP_P4/. MIT-P08 is within the paper (Li et al., 2008) and its supporting information. The S-wave tomography model SEMUCB-WM1 is available is at http://seismo.berkeley.edu/wiki_br/. S40RTS is available at https://jritsema.earth.lsa.umich.edu/Research.html.

Appendix A. Supplementary data

Supplementary data to this article can be found online at https://doi.org/10.1016/j.earscirev.2023.104414.

References

Amaru, M., 2007. Global Travel Time Tomography with 3-D Reference Models. Utrecht Univ, Geologica Ultraiectina.

Billen, M.I., Hirth, G., 2005. Newtonian versus non-Newtonian upper mantle viscosity: implications for subduction initiation. Geophys. Res. Lett. 32, 1–4. https://doi.org/10.1029/2005GL023457.

Bird, P., 1988. Formation of the Rocky Mountains, Western United States: a continuum computer model. Science 239, 1501–1507. https://doi.org/10.1126/science.239.4847.1501.

Bower, D.J., Gurnis, M., Flament, N., 2015. Assimilating lithosphere and slab history in 4-D Earth models. Phys. Earth Planet. Inter. 238, 8–22. https://doi.org/10.1016/j.pepi.2014.10.013.

Bunge, H.P., Richards, M.A., Baumgardner, J.R., 2002. Mantle-circulation models with sequential data assimilation: inferring present-day mantle structure from plate-motion histories. Philos. Trans. R. Soc. A Math. Phys. Eng. Sci. 360, 2545–2567. https://doi.org/10.1098/rsta.2002.1080.

Bunge, H.P., Richards, M.A., Lithgow-Bertelloni, C., Baumgardner, J.R., Grand, S.P., Romanowicz, B.A., 1998. Time scales and heterogeneous structure in geodynamic earth models. Science 280, 91–95. https://doi.org/10.1126/science.280.5360.91.

Chang, S.J., Ferreira, A.M.G., Faccenda, M., 2016. Upper- and mid-mantle interaction between the Samoan plume and the Tonga-Kermadec slabs. Nat. Commun. 7, 10799. https://doi.org/10.1038/ncomms10799.

Chertova, M.V., Spakman, W., Steinberger, B., 2018. Mantle flow influence on subduction evolution. Earth Planet. Sci. Lett. 489, 258–266. https://doi.org/10.1016/j.epsl.2018.02.038.

Christensen, U.R., 1996. The influence of trench migration on slab penetration into the lower mantle. Earth Planet. Sci. Lett. 140, 27–39. https://doi.org/10.1016/0012-821X(96)00023-4.

Christensen, U.R., Yuen, D.A., 1985. Layered convection induced by phase transitions. J. Geophys. Res. 90, 10291. https://doi.org/10.1029/JB090iB12p10291.

Coney, P.J., Reynolds, S.J., 1977. Cordilleran Benioff zones. Nature 270, 403–406. https://doi.org/10.1038/270403a0.

Contenti, S., Gu, Y.J., Ökeler, A., Sacchi, M.D., 2012. Shear wave reflectivity imaging of the Nazca-South America subduction zone: stagnant slab in the mantle transition zone? Geophys. Res. Lett. 39, n/a-n/a. https://doi.org/10.1029/2011GL050064.

Davies, D.R., Goes, S., Davies, J.H., Schuberth, B.S.A., Bunge, H.P., Ritsema, J., 2012. Reconciling dynamic and seismic models of Earth's lower mantle: the dominant role of thermal heterogeneity. Earth Planet. Sci. Lett. 353–354, 253–269. https://doi.org/10.1016/j.epsl.2012.08.016.

Druken, K.A., Kincaid, C., Griffiths, R.W., Stegman, D.R., Hart, S.R., 2014. Plume-slab interaction: the Samoa-Tonga system. Phys. Earth Planet. Inter. 232, 1–14. https://doi.org/10.1016/j.pepi.2014.03.003.

England, P., Houseman, G., 1986. Finite strain calculations of continental deformation: 2. Comparison with the India-Asia Collision Zone. J.Geophys.Res.Solid Earth 91, 3664–3676. https://doi.org/10.1029/JB091iB03p03664.

English, J.M., Johnston, S.T., Wang, K., 2003. Thermal modelling of the Laramide orogeny: ţesting the flat-slab subduction hypothesis. Earth Planet. Sci. Lett. 214, 619–632. https://doi.org/10.1016/S0012-821X(03)00399-6.

Espurt, N., Funiciello, F., Martinod, J., Guillaume, B., Regard, V., Faccenna, C., Brusset, S., 2008. Flat subduction dynamics and deformation of the South American plate: insights from analog modeling. Tectonics 27, 1–19. https://doi.org/10.1029/2007TC002175.

Faccenna, C., Oncken, O., Holt, A.F., Becker, T.W., 2017. Initiation of the Andean orogeny by lower mantle subduction. Earth Planet. Sci. Lett. 463 https://doi.org/10.1016/j.epsl.2017.01.041.

Flament, N., 2019. Present-day dynamic topography and lower-mantle structure from palaeogeographically constrained mantle flow models. Geophys. J. Int. 216, 2158–2182. https://doi.org/10.1093/gji/ggy526.

French, S.W., Romanowicz, B.A., 2014. Whole-mantle radially anisotropic shear velocity structure from spectral-element waveform tomography. Geophys. J. Int. 199, 1303–1327. https://doi.org/10.1093/gji/ggu334.

Fukao, Y., Obayashi, M., Inoue, H., Nenbai, M., 1992. Subducting slabs stagnant in the mantle transition zone. J. Geophys. Res. 97, 4809–4822. https://doi.org/10.1029/91JB02749.

Gerya, T.V., Bercovici, D., Becker, T.W., 2021. Dynamic slab segmentation due to brittle–ductile damage in the outer rise. Nature 599, 245–250. https://doi.org/10.1038/s41586-021-03937-x.

Goes, S., Agrusta, R., van Hunen, J., Garel, F., 2017. Subduction-transition zone interaction: a review. Geosphere 13, 644–664. https://doi.org/10.1130/GES01476.1.

Grand, S.P., van der Hilst, R.D., Widiyantoro, S., 1997. Global seismic tomography: a snapshot of convection in the Earth. GSA Today 7, 1–7.

Gurnis, M., Hager, B.H., 1988. Controls of the structure of subducted slabs. Nature 335, 317–321. https://doi.org/10.1038/335317a0.

Gurnis, M., Müller, R.D., Moresi, L., 1998. Cretaceous vertical motion of Australia and the AustralianAntarctic discordance. Science 279, 1499–1504. https://doi.org/10.1126/science.279.5356.1499.

Gutscher, M.A., Spakman, W., Bijwaard, H., Engdahl, E.R., 2000. Geodynamics of flat subduction: Seismicity and tomographic constraints from the andean margin. Tectonics 19, 814–833. https://doi.org/10.1029/1999TC001152.

Han, L., Gurnis, M., 1999. How valid are dynamic models of subduction and convection when plate motions are prescribed? Phys. Earth Planet. Inter. 110, 235–246. https://doi.org/10.1016/S0031-9201(98)00156-3.

Hassan, R., Müller, R.D., Gurnis, M., Williams, S.E., Flament, N., 2016. A rapid burst in hotspot motion through the interaction of tectonics and deep mantle flow. Nature 533, 239–242. https://doi.org/10.1038/nature17422.

Heller, P.L., Liu, L., 2016. Dynamic topography and vertical motion of the U.S. Rocky Mountain region prior to and during the Laramide orogeny. Bull. Geol. Soc. Am. 128, 973–988. https://doi.org/10.1130/B31431.1.

Hu, J., Liu, L., 2016. Abnormal seismological and magmatic processes controlled by the tearing South American flat slabs. Earth Planet. Sci. Lett. 450, 40–51. https://doi.org/10.1016/j.epsl.2016.06.019.

Hu, J., Liu, L., Gurnis, M., 2021. Southward expanding plate coupling due to variation in sediment subduction as a cause of andean growth. Nat. Commun. 12 https://doi.org/10.1038/s41467-021-27518-8.

Hu, J., Liu, L., Hermosillo, A., Zhou, Q., 2016. Simulation of late Cenozoic South American flat-slab subduction using geodynamic models with data assimilation. Earth Planet. Sci. Lett. 438, 1–13. https://doi.org/10.1016/j.epsl.2016.01.011.

Hu, J.S., Liu, L.J., Zhou, Q., 2018. Reproducing past subduction and mantle flow using high-resolution global convection models. Earth Planet. Phys. 2, 189–207. https://doi.org/10.26464/epp2018019.

Huang, J., Zhao, D., 2006. High-resolution mantle tomography of China and surrounding regions. J. Geophys.Res.Solid Earth 111, 1–21. https://doi.org/10.1029/2005JB004066.

Humphreys, E.D., 1995. Post-Laramide removal of the Farallon slab, western United States. Geology 23, 987–990. https://doi.org/10.1130/0091-7613(1995)023<0987:PLROTF>2.3.CO;2.

Ismail-Zadeh, A., Schubert, G., Tsepelev, I., Korotkii, A., 2004. Inverse problem of thermal convection: numerical approach and application to mantle plume restoration. Phys. Earth Planet. Inter. 145, 99–114. https://doi.org/10.1016/j.pepi.2004.03.006.

Jones, C., 2012. Hydrodynamic mechanism for the Laramide orogeny. Geosphere 7, 183. https://doi.org/10.1130/GES00575.1.

Jordán, T.E., Isacks, B.L., Allmendinger, R.W., Brewer, J.A., Ramos, V.A., Ando, C.J., 1983. Andean tectonics related to geometry of subducted Nazca plate. Geol. Soc. Am. Bull. 94, 341. https://doi.org/10.1130/0016-7606(1983)94<341:ATRTGO>2.0.CO;2.

King, S.D., Frost, D.J., Rubie, D.C., 2015. Why cold slabs stagnate in the transition zone. Geology 43, 231–234. https://doi.org/10.1130/G36320.1.

Lau, H.C.P., Mitrovica, J.X., Davis, J.L., Tromp, J., Yang, H.Y., Al-Attar, D., 2017. Tidal tomography constrains Earth's deep-mantle buoyancy. Nature 551, 321–326. https://doi.org/10.1038/nature24452.

Leng, W., Gurnis, M., 2015. Subduction initiation at relic arcs. Geophys. Res. Lett. 42, 7014–7021. https://doi.org/10.1002/2015GL064985.

Li, C., Van Der Hilst, R.D., Engdahl, E.R., Burdick, S., 2008. A new global model for P wave speed variations in Earth's mantle. Geochem. Geophys. Geosyst. 9 https://doi.org/10.1029/2007GC001806.

Li, J., Zhang, Y., Dong, S., Johnston, S.T., 2014. Cretaceous tectonic evolution of South China: a preliminary synthesis. Earth Sci. Rev. 134, 98–136. https://doi.org/10.1016/j.earscirev.2014.03.008.

Li, X.H., 2000. Cretaceous magmatism and lithospheric extension in Southeast China. J. Asian Earth Sci. 18, 293–305. https://doi.org/10.1016/S1367-9120(99)00060-7.

Liu, L., 2015. The ups and downs of North America: evaluating the role of mantle dynamic topography since the Mesozoic. Rev. Geophys. 53, 1022–1049. https://doi.org/10.1002/2015RG000489.

Liu, L., 2014. Constraining cretaceous subduction polarity in eastern Pacific from seismic tomography and geodynamic modeling. Geophys. Res. Lett. 41, 8029–8036. https://doi.org/10.1002/2014GL061988.

Liu, L., Spasojević, S., Gurnis, M., 2008. Reconstructing Farallon plate subduction beneath North America back to the Late Cretaceous. Science 322, 934–938. https://doi.org/10.1126/science.1162921.

Liu, L., Stegman, D.R., 2011. Segmentation of the Farallon slab. Earth Planet. Sci. Lett. 311, 1–10. https://doi.org/10.1016/j.epsl.2011.09.027.

Liu, L., Gurnis, M., 2008. Simultaneous Inversion of Mantle Properties and Initial Conditions Using an Adjoint of Mantle Convection. J. Geophy. Res. 113, B08405. https://doi.org/10.1029/2008JB005594.

Liu, Liang, Liu, Lijun, Xu, Y.G., 2021. Mesozoic intraplate tectonism of East Asia due to flat subduction of a composite terrane slab. Earth Sci. Rev. 214, 103505 https://doi.org/10.1016/j.earscirev.2021.103505.

Liu, Lijun, Peng, D., Liu, Liang, Chen, L., Li, S., Wang, Y., Cao, Z., Feng, M., 2021. East Asian lithospheric evolution dictated by multistage Mesozoic flat-slab subduction. Earth Sci. Rev. 217, 103621 https://doi.org/10.1016/j.earscirev.2021.103621.

Ma, P., Liu, S., Gurnis, M., Zhang, B., 2019. Slab horizontal subduction and slab tearing beneath East Asia. Geophys. Res. Lett. 46, 5161–5169. https://doi.org/10.1029/2018GL081703.

Mao, W., Zhong, S., 2018. Slab stagnation due to a reduced viscosity layer beneath the mantle transition zone. Nat. Geosci. 11, 876–881. https://doi.org/10.1038/s41561-018-0225-2.

McNamara, A.K., 2019. A review of large low shear velocity provinces and ultra low velocity zones. Tectonophysics 760, 199–220. https://doi.org/10.1016/j.tecto.2018.04.015.

McNamara, A.K., Zhong, S., 2004. Thermochemical structures within a spherical mantle: superplumes or piles? J. Geophys.Res.Solid Earth 109, 1–14. https://doi.org/10.1029/2003JB002847.

Müller, R.D., Seton, M., Zahirovic, S., Williams, S.E., Matthews, K.J., Wright, N.M., Shephard, G.E., Maloney, K.T., Barnett-Moore, N., Hosseinpour, M., Bower, D.J., Cannon, J., 2016. Ocean basin evolution and global-scale plate reorganization events since Pangea Breakup. Annu. Rev. Earth Planet. Sci. 44, 107–138. https://doi.org/10.1146/annurev-earth-060115-012211.

Obayashi, M., Yoshimitsu, J., Nolet, G., Fukao, Y., Shiobara, H., Sugioka, H., Miyamachi, H., Gao, Y., 2013. Finite frequency whole mantle P wave tomography: improvement of subducted slab images. Geophys. Res. Lett. 40, 5652–5657. https://doi.org/10.1002/2013GL057401.

Pang, M., Nummedal, D., 1995. Flexural subsidence and basement tectonics of the Cretaceous Western Interior Basin, United States. Geology 23, 173–176. https://doi.org/10.1130/0091-7613(1995)023<0173:FSABTO>2.3.CO;2.

Peng, D., Liu, L., 2022. Quantifying slab sinking rates using global geodynamic models with data-assimilation. Earth Sci. Rev. 230, 104039 https://doi.org/10.1016/j.earscirev.2022.104039.

Peng, D., Liu, L., Hu, J., Li, S., Liu, Y., 2021. Formation of East Asian stagnant slabs due to a pressure-driven cenozoic mantle wind following mesozoic subduction. Geophys. Res. Lett. 48, 1–10. https://doi.org/10.1029/2021GL094638.

Peng, D., Liu, L., Wang, Y., 2021b. A newly discovered Late-Cretaceous East Asian Flat Slab explains its unique lithospheric structure and tectonics. J. Geophys.Res.Solid Earth 126, 1–23. https://doi.org/10.1029/2021JB022103.

Portner, D.E., Rodríguez, E.E., Beck, S., Zandt, G., Scire, A., Rocha, M.P., Bianchi, M.B., Ruiz, M., França, G.S., Condori, C., Alvarado, P., 2020. Detailed structure of the subducted Nazca slab into the Lower Mantle derived from continent-scale teleseismic P wave tomography. J.Geophys.Res.Solid Earth 125, 1–26. https://doi.org/10.1029/2019JB017884.

Pusok, A.E., Stegman, D.R., 2020. The convergence history of India-Eurasia records multiple subduction dynamics processes. Sci. Adv. 6 https://doi.org/10.1126/sciadv.aaz8681.

Reiss, M.C., Long, M.D., Creasy, N., 2019. Lowermost Mantle Anisotropy beneath Africa from differential SKS-SKKS shear-wave splitting. J.Geophys.Res.Solid Earth 124, 8540–8564. https://doi.org/10.1029/2018JB017160.

Ritsema, J., Deuss, A., Van Heijst, H.J., Woodhouse, J.H., 2011. S40RTS: a degree-40 shear-velocity model for the mantle from new Rayleigh wave dispersion, teleseismic traveltime and normal-mode splitting function measurements. Geophys. J. Int. 184, 1223–1236. https://doi.org/10.1111/j.1365-246X.2010.04884.x.

Saleeby, J., 2003. Segmentation of the Laramide Slab - evidence from the southern Sierra Nevada region. Bull. Geol. Soc. Am. 115, 655–668. https://doi.org/10.1130/0016-7606(2003)115<0655:SOTLSF>2.0.CO;2.

Schellart, W.P., Freeman, J., Stegman, D.R., Moresi, L., May, D., 2007. Evolution and diversity of subduction zones controlled by slab width. Nature 446, 308–311. https://doi.org/10.1038/nature05615.

Schuberth, B.S.A., Bunge, H.P., 2009. Tomographic filtering of high-resolution mantle circulation models: can seismic heterogeneity be explained by temperature alone? Geochem. Geophys. Geosyst. 10 https://doi.org/10.1029/2009GC002401.

Sigloch, K., Mihalynuk, M.G., 2013. Intra-oceanic subduction shaped the assembly of Cordilleran North America. Nature 496, 50–56. https://doi.org/10.1038/nature12019.

Stegman, D.R., Freeman, J., Schellart, W.P., Moresi, L., May, D., 2006. Influence of trench width on subduction hinge retreat rates in 3-D models of slab rollback. Geochem. Geophys. Geosyst. 7 https://doi.org/10.1029/2005GC001056.

Strak, V., Schellart, W.P., 2014. Evolution of 3-D subduction-induced mantle flow around lateral slab edges in analogue models of free subduction analysed by stereoscopic particle image velocimetry technique. Earth Planet. Sci. Lett. 403, 368–379. https://doi.org/10.1016/j.epsl.2014.07.007.

Tan, E., Choi, E., Thoutireddy, P., Gurnis, M., Aivazis, M., 2006. GeoFramework: coupling multiple models of mantle convection within a computational framework. Geochem. Geophys. Geosyst. 7, 1–14. https://doi.org/10.1029/2005GC001155.

Torsvik, T.H., Müller, R.D., Van Der Voo, R., Steinberger, B., Gaina, C., 2008. Global plate motion frames: toward a unified model. Rev. Geophys. 46 https://doi.org/10.1029/2007RG000227.

van der Hilst, R., Seno, T., 1993. Effects of relative plate motion on the deep structure and penetration depth of slabs below the Izu-Bonin and Mariana island arcs. Earth Planet. Sci. Lett. 120, 395–407. https://doi.org/10.1016/0012-821X(93)90253-6.

van der Meer, D.G., Spakman, W., van Hinsbergen, D.J.J., Amaru, M.L., Torsvik, T.H., 2010. Towards absolute plate motions constrained by lower-mantle slab remnants. Nat. Geosci. 3, 36–40. https://doi.org/10.1038/ngeo708.

Wu, F.-Y., Yang, J.-H., Xu, Y.-G., Wilde, S.A., Walker, R.J., 2019. Destruction of the North China Craton in the Mesozoic. Annu. Rev. Earth Planet. Sci. 47, 173–195. https://doi.org/10.1146/annurev-earth-053018-060342.

Yang, T., Moresi, L., Gurnis, M., Liu, S., Sandiford, D., Williams, S., Capitanio, F.A., 2019. Contrasted East Asia and South America tectonics driven by deep mantle flow. Earth Planet. Sci. Lett. 517, 106–116. https://doi.org/10.1016/j.epsl.2019.04.025.

Yin, A., 2010. Cenozoic tectonic evolution of Asia: a preliminary synthesis. Tectonophysics 488, 293–325. https://doi.org/10.1016/j.tecto.2009.06.002.

Zhang, N., Li, Z.-X., 2018. Formation of mantle "lone plumes" in the global downwelling zone — a multiscale modelling of subduction-controlled plume generation beneath the South China Sea. Tectonophysics 723, 1–13. https://doi.org/10.1016/j.tecto.2017.11.038.

Zhong, S., Gurnis, M., 1995. Mantle convection with plates and mobile, faulted plate margins. Science 267, 838–843. https://doi.org/10.1126/science.267.5199.838.

Zhong, S., McNamara, A., Tan, E., Moresi, L., Gurnis, M., 2008. A benchmark study on mantle convection in a 3-D spherical shell using CitcomS. Geochem. Geophys. Geosyst. 9, 1–32. https://doi.org/10.1029/2008GC002048.

Zhong, S., Zhang, N., Li, Z.X., Roberts, J.H., 2007. Supercontinent cycles, true polar wander, and very long-wavelength mantle convection. Earth Planet. Sci. Lett. 261, 551–564. https://doi.org/10.1016/j.epsl.2007.07.049.

Zhou, Q., Liu, L., 2017. A Hybrid Forward-Adjoint Data Assimilation Approach for Reconstructing the Temporal Evolution of Mantle Dynamics. Geochem. Geophy. Geosys. 18 https://doi.org/10.1002/2017GC007116.

Zhou, Q., Liu, L., Hu, J., 2018. Western US volcanism due to intruding oceanic mantle driven by ancient Farallon slabs. Nat. Geosci. 11, 70–76. https://doi.org/10.1038/s41561-017-0035-y.